List of papers

This thesis is based on the following publications:

1. Banse X, Devogelaer J P, Munting E, Delloye C, Cornu O, Grynpas M D. Inhomogeneity of human vertebral cancellous bone. Systematic density and structure patterns inside the vertebral body. Bone 2001; 28 (5): 563-71.

2. Banse X, Devogelaer J P, Grynpas M. Patient specific micro-architecture of the vertebral cancellous bone: A pQCT and histological study. Bone 2002a; (In press).

3. Banse X, Lafosse A, Grynpas M, Bailey A J. The cross-link profile of bone collagen correlates with the structural organization of the trabeculae. Bone 2002b; (In press).

4. Banse X, Sims T J, Bailey A J. Mechanical properties of adult vertebral cancellous bone: Correlation with collagen intermolecular cross-links. J Bone Miner Res 2002c; (In press).

5. Banse X, Devogelaer J P. Does the pQCT ignore the tissue density? J Clin Densitom 2002; (In press).

Structure of the thesis

This review is the report of a single experimental protocol on the nature, structure and mechanical strength of 136 bone samples from the vertebral body of 9 subjects. On these samples, we combined mechanical testing with density measurements (part I), a study of some microarchitectural parameters (part II) and a biochemical analysis of bone collagen (part III). As multiple samples were studied in each subject we explored whether a given parameter was characteristic of that subject. The parameters were also systematically screened as potential indicators of the bone quality. The association of biochemical and microarchitectural data offered a unique opportunity to compare both sets of data (part IV). Finally, in a technical addendum, we report the comparison of histology vs pQCT (a small scanner) as investigation tools for the bone density and microarchitecture.

Part I: Density and mechanics, patient-specific discrepancy

Introduction

Osteoporosis and vertebral fracture

Osteoporosis is defined as a 'systemic skeletal disease characterized by low bone mass and microarchitectural deterioration of bone tissue, leading to enhanced bone fragility and a consequent increase in bone fracture risk' (Consensus development conference 1993). The definition itself contains the natural history of the disease. Some physical properties of the bone are altered (low bone mass, compromised microarchitecture…) leading to reduced mechanical properties ('bone fragility') and increased fracture risk.

The term 'fragility fractures' refers to fractures that occur in response to minor trauma that are part of everyday life (like fall, coughing…). The continuous increase of life expectancy has made osteoporosis a major public health issue. For the American woman, the estimated lifetime risk of sustaining a distal forearm (Colles) fracture is 16.0%; for the hip fracture, this risk is 17%, and for *symptomatic* vertebral compressive fracture the risk is 15.6% (Melton et al. 1992). Fractures may occur at other skeletal sites: proximal humerus, sternum, rib, pelvis, hand, clavicule, foot… (Seeley et al. 1991). Although not comparable to the morbidity of the hip fracture (that necessitates surgery and hospitalization) the occurrence of vertebral crush fracture (Figure 1) is associated with a significant rate of hospitalization (Jacobsen et al. 1992), and reduction in the 5 year survival rate (Cooper et al. 1993). Intra- and extra-osseous factors contribute to the fracture risk. Extra-osseous factors include impaired reflexes, insufficient soft tissue covering and environmental hazards. Intra-osseous factors refer to reduced mechanical properties of the skeletal element itself (Figure 2).

BMD and non-BMD factors

Today's diagnosis of osteoporosis mainly relies on bone mass measurement. The bone mineral density (BMD) as measured by modern investigation tools used for densitometry (SPA, DXA, QCT…), declines with age and this decline is associated with an increased fracture risk (Genant et al. 1996). However the use of this single parameter to predict the fracture risk has some limitations. For a same BMD value, there is a significant overlap between patients that underwent fracture and those who did not (Recker 1993). Fracture may occur in patients with 'normal' BMD and be absent in patients with low BMD.

Clinical evidence of the skeletal fragility arising from factors others than BMD has been reported by Ross et al. (1991). They showed that patients with one or more spinal fractures but high BMD were much more likely to suffer from subsequent fracture than those without prior fracture and with low BMD. Those who fractured demonstrated that they had a basis for fragility that was distinct from, and in addition to, a reduced BMD. Finally, quantitative ultrasonography recently appeared as having

Figure 1. Osteoporotic patient presenting a typical compressive fracture of the L1 level.

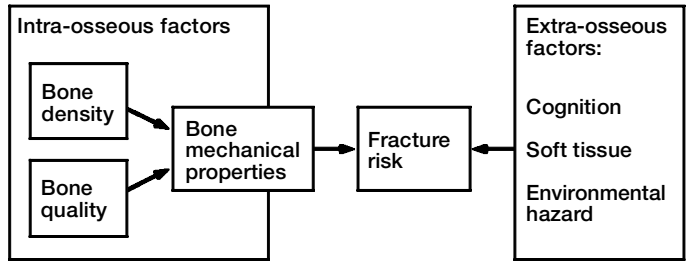

Figure 2. Intra and extra-osseous factors that may affect the fracture risk.

predictive capability of fracture risk, independent of the BMD measurement, meaning that ultrasonography actually measures something else than the bone mass (Gluer et al. 1996).

Regarding the intrinsic properties of bone (Figure 2), we will consider that the BMD or apparent density is a reflection of the bone quantity, while the non-BMD factors affecting the mechanical properties of the skeleton will be referred to as indicators of the bone quality (Heaney 1993). The above mentioned clinical observations lead to the hypothesis that different patients had different bone quality.

In vitro studies: bone density and bone quality

Compared to the clinical studies, laboratory investigations have the major advantage to rule out the extra-osseous factors and directly focus on the relationship between mechanical and other physical properties of a skeletal element.

Previous studies have shown that the load-bearing capacity of the vertebral body was partially dependent on its size (Mosekilde 1986) and partially on the thickness of its thin cortical shell (McBroom et al. 1985). But most of all, it depends on the mechanical properties of its main constituent: the *cancellous bone* (Jiang et al. 1998; Singer et al. 1995). There is now strong evidence that the mechanical competence of this material is mainly related to its density. This was shown for cancellous bone from various anatomic sites (McCalden et al. 1997; Linde et al. 1992) and, more specifically, for the vertebral cancellous bone (Kopperdahl and Keaveny 1998; Mosekilde and Danielsen 1987; Hansson et al. 1987; Lindahl 1976; Bell et al. 1967). However, a substantial part of the variance of the mechanical properties (typically 20 to 30%) remained unaccountable by the density. The laboratory counterpart of the clinical concept of bone quality should be found in this scattering. The *quality* of a sample is the part of variance in the mechanical properties that is not explained by the density. If different subjects (or patients) have different *bone quality*, the fact that a bone sample comes from a given subject should systematically affect the relationship between density and mechanical properties. However, to our knowledge, this has not yet been demonstrated.

Material and methods

Origin of the material

The vertebral bodies of the lower spine were harvested by section of the pedicles during autopsy from nine donors without any known bone or metastatic disorder. Median age was 60 (44–88) years, three donors were females and six were males. The protocol was authorized by the local ethics committee. Each donor (or patient) was identified as an individual ***subject*** (A, B……to I) in this work.

Coring the samples

Vertebral bodies were obtained at different ***vertebral levels***: from the lower *thoracic* spine (T9), *thoraco-lumbar* junction (either T12 or L1) or low *lumbar* spine (L4). They were stripped of all soft tissues including the intervertebral discs and checked further for any obvious bone lesion by radiography. Cylindrical samples (8.2 mm diameter) were vertically cored from each subject: two in the T9 vertebral body, three in the T12 or L1 and three in the L4. Location within the vertebral body (***coring site***) was either anterior (Ant.), posterior (Post.) or external (Ext., Figure 3). The procedure was performed under water using a diamond tipped coring tool (Starlite, Rosemont, PA). Such a tool has been shown to limit the damage to the

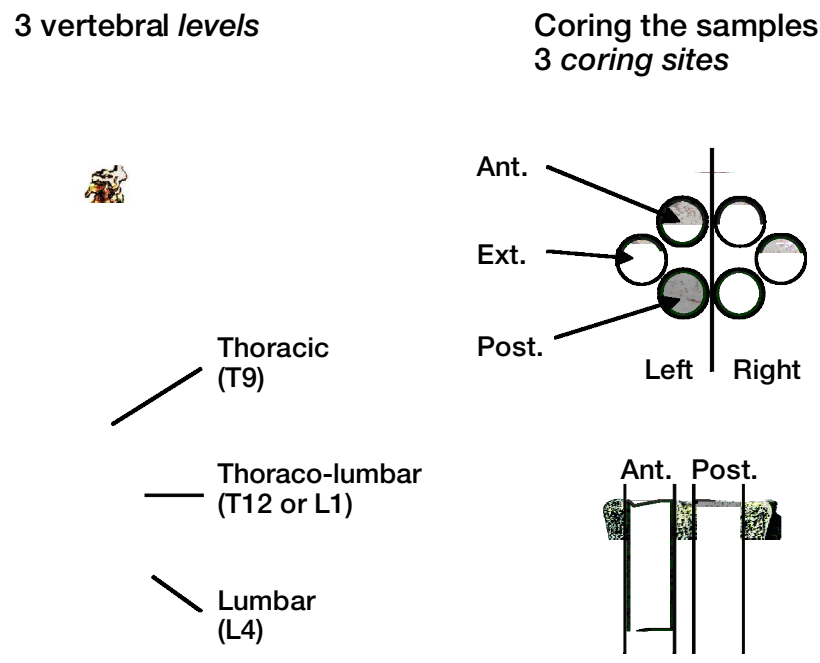

Figure 3. Cylindrical samples (diameter: 8.2 mm) were vertically cored in the vertebral bodies from nine subjects. The origin of a sample was defined by the name of the individual subject and two locations variable: the vertebral level in the spine and the sample site of coring. Usually, two samples (one anterior and one posterior) were cored in the thoracic level (T9), and three samples (one anterior, one posterior and one external) in the thoraco lumbar (T12 or L1) and lumbar (L4) levels for a total of 16 samples in a single subject.

very thin, fragile trabeculae of the cancellous bone, grinding the material instead of cutting it (Keaveny et al. 1994). There was no cortical shell in the cores.

In one T12 specimen the external sample was not obtained and in one subject the L4 vertebral body was discarded because, during coring, two samples from that vertebra presented signs of unexpected necrosis and subsequent over-mineralization. This resulted in a cohort of 136 cylindrical samples of vertebral cancellous bone. End-plates were left in place and the total length of the samples was measured using a digital caliper (L_T: 19–29 mm). Cylinders were placed in plastic vials fitting their diameter, oriented and labeled before storage at –30º C. The bone marrow was left in place.

Density measurement: pQCT acquisition

All the samples were scanned using a pQCT scanner (for 'Peripheral Quantitative Computed Tomography). This machine (pQCT Research SA+® Stratec, Pforzheim, Germany) is a small X-ray CT scan based on the translation-rotation principle and originally designed to quantify repeatedly the mineral density of small animals. The pQCT produces images of a relatively good quality (see addendum), allowing a correct assessment of the morphometry. However, for this part of the study it was only used for density measurements, resulting from four transverse slices obtained from bottom to top of the cylinder. The bone mineral density (mgHA/cm³) was calculated by the pQCT and directly converted to ***density*** values (g/cm³). The validation of such conversion is detailed in the addendum.

Mechanical testing

Before mechanical testing a random number was assigned to each of the 136 samples and the tests were performed using this random order to reduce the risk of bias that would influence a group of samples.

Specimen mounting was performed according to a validated method that minimizes the end-artifacts

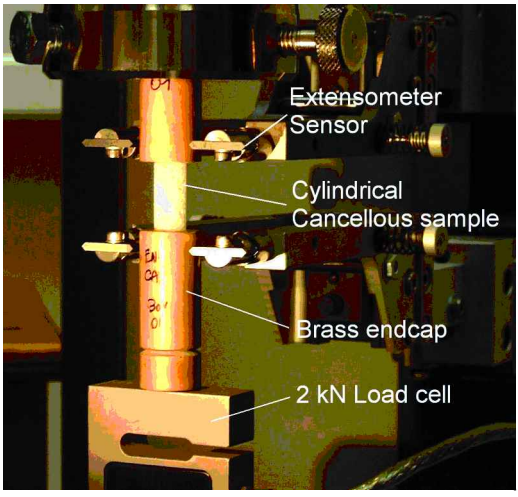

Figure 4. The samples were glued in supporting brass 'endcaps' and tested in compression. Strains were estimated by measuring the displacement between the upper and lower supporting endcap. Forces were recorded using a 2kN load cell.

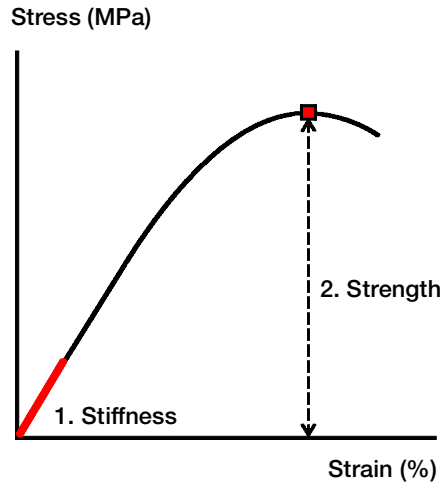

Figure 5. Typical stress-strain curve

(Kopperdahl et al. 1999; Kopperdahl and Keaveny 1998; Keaveny et al. 1997). Before mechanical testing the cancellous cylindrical samples were fixed on both upper and lower ends into brass cylinders (called 'endcap', diameter 13mm). These supports have a 8.3 mm hole that was threaded internally. Both ends of the bone samples were prepared (gently washed with water and briefly dehydrated in methanol) over a length of 5 mm, leaving in place the marrow in the middle portion of the sample. The samples were then inserted in the endcap in which the inner-threaded surface had been covered with cyanoacrylate (Loctite 401®). During the insertion the alignment between the specimen and the endcap axis was ensured by performing the procedure on a precision V-block. After mounting both ends, the exposed length was measured twice with a caliper. The effective gauge length (H0, mm) was calculated as: [(L_T + exposed length) / 2], considering that half of the 'end-capped' material is not effectively tested (Keaveny et al. 1997). The specimens were rehydrated in normal saline for four hours at room temperature in protective plastic vials until mechanical testing.

Uniaxial compressive tests (Figure 4) were performed at room temperature on a computer controlled screw driven testing machine (Zwick model Z50/TH3A, Ulm - Germany). The forces were measured with a 2kN load cell and deformations were recorded with a Multisens extensometer (Zwick, Ulm, Germany). The strain (%) was calculated as the deformation (mm) divided by H0 (mm). No preconditioning cycles were performed since (contrary to the classical platens test) their utility was not demonstrated with the 'endcap technique' where there is no detectable positioning of the sample (Keaveny et al. 1999). The strain-rate was 0.001 s^{-1} and the loading was stopped at 2% strain. Three specimens were loaded incorrectly and for three other tests data were lost due to operator error, leaving 130 successfully tested specimens.

Mechanical parameters were calculated from the stress-strain curve (Figure 5). The ***stiffness*** (MPa) was calculated by linear regression of the stress-strain curve between 0.001% and 0.2 % strain. The ultimate point was defined as the point where the slope of the stress-strain curve was zero (the point of maximum stress). The ***strength*** (MPa) was the stress at the ultimate point.

Statistical analysis

The data were explored with SPSS 10.0 (SPSS Inc., Chicago, IL). Simple correlation was used to estimate the overall prediction of the mechanical parameters by the apparent density.

To investigate the influence of the factors *subject*, vertebral *level* and *coring site* on the mechanical parameters, we used a mixed model. This

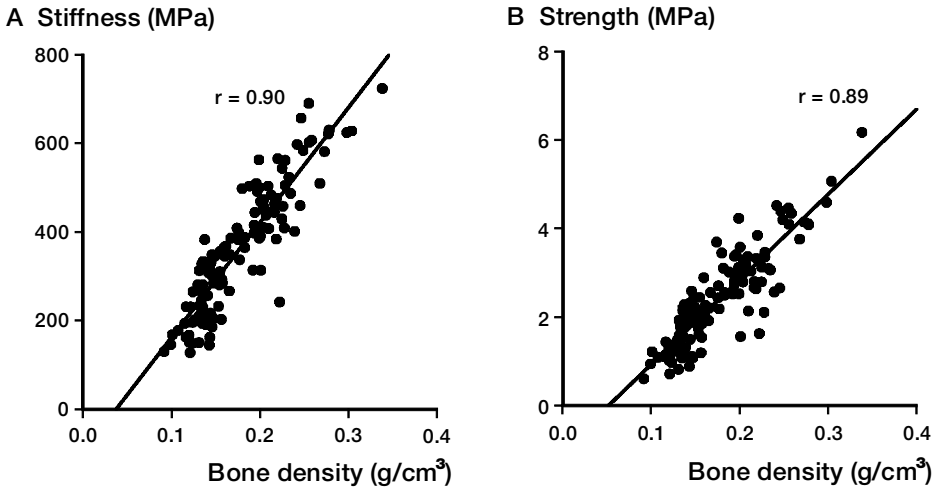

Figure 6. Both stiffness (A) and strength (B) were correlated to the density.

model is analog to a repeated measure analysis of variance. The subject was introduced as a random factor, to estimate if the differences between the subjects were significant. The location variables (vertebral level and coring site) were introduced as fixed factor, meaning that the differences between levels and coring sites were considered as equal in each subject, the usual assumption in analysis of variance. We tested the factors (*subjects*, *level* and coring *site*) using a F-test. Estimated marginal means (± standard error, SE) were obtained for each group of variables and compared (when needed) using post-hoc pairwise comparison with Bonferroni adjustment. When mentioned in the text, differences were always significant ($p < 0.01$) and expressed as percentage of the mean value.

To know whether the relationship between mechanics and density varied among different subjects or locations, we ran the same model but, adding the density as covariable (random regression model, a model analog to an ANCOVA model). Then we checked if the introduction of this covariate, the density, was able to control the differences between subjects or location variables.

Results

For the whole set of samples

The cylinders had relatively low density (0.09–0.37 g/cm³), low stiffness (127–725 MPa) and low strength (0.60–6.17 MPa), covering a wide range of values. The stiffness (Figure 6A) and strength (Figure 6B) were directly correlated to the density.

Differences between subject and locations

The various parameters were different among the subjects (Figure 7). They had different density ($p < 0.001$), different stiffness ($p < 0.001$, Figure 8 A) and different strength ($p < 0.001$, Figure 8 C). For some subjects the stiffness and strength were three times higher than for others (i.e. compare subject B and subject E).

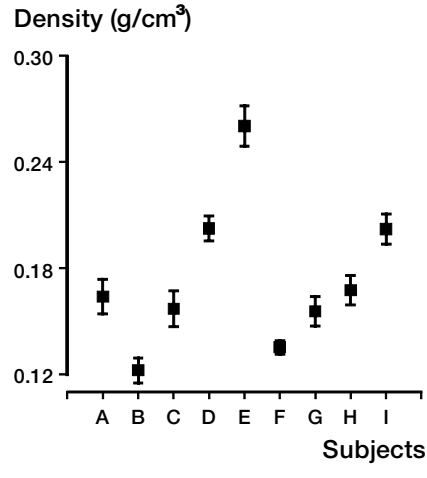

Figure 7. variations of the density among 9 patients (A to I). The marker indicates the estimated marginal mean, and the error bar represents ± 1 SE for that estimate.

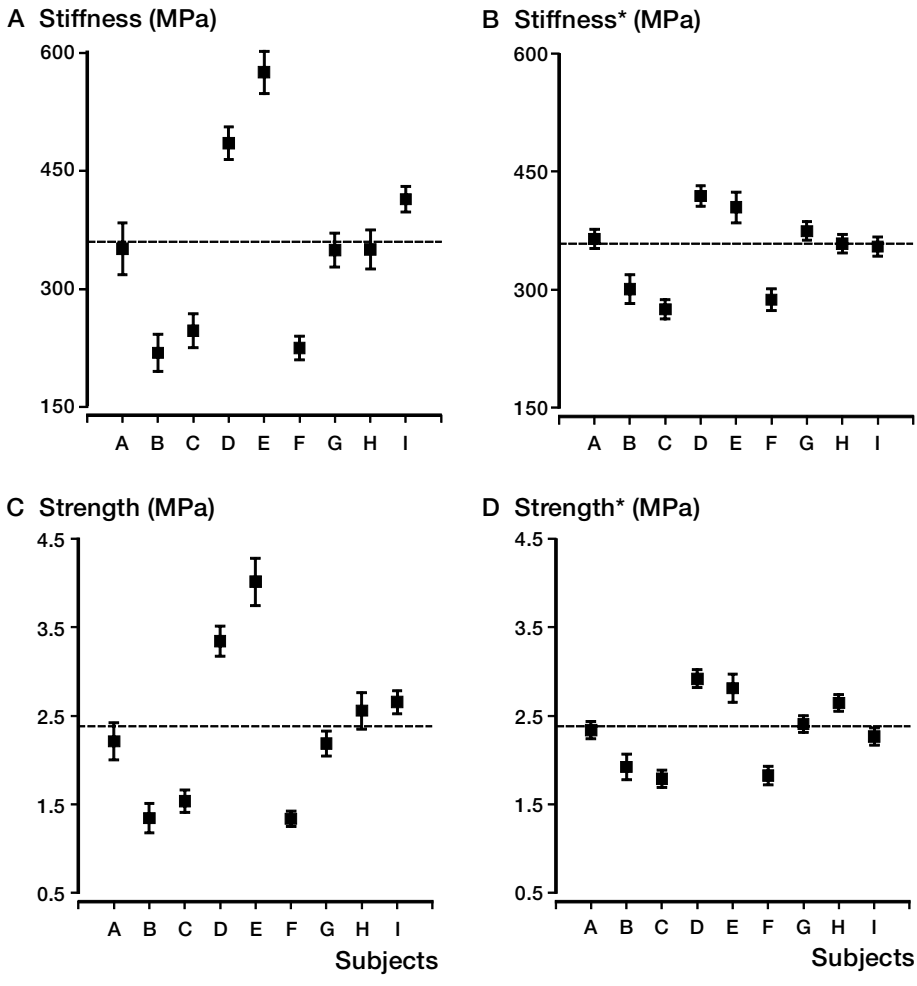

Figure 8. Variation of the stiffness and strength among patients. Most of the differences are linked to differences in sample's density (see fig. 7). The stiffness and strength of the cancellous bone varied among subjects (8 A and 8 C). When correcting the values for density (8 B and 8 D, as indicated by *), substantial differences in mechanical properties persisted. This demonstrates that, after accounting for the density some subjects (D and E) had 40% stronger and stiffer bone than others (C and F). Some subject had higher or lower 'bone quality'.

The mixed model showed that cylinders from the anterior and external coring *site* were ~21% less dense than those from the posterior site (Table 1). Additionally, the samples from the lumbar vertebra were ~10% less dense than those coming from the thoraco-lumbar and thoracic vertebral bodies. The stiffness and strength values of the anterior samples were ~25% lower than the posterior. The largest differences were observed when comparing the posterior with the external samples (~40%). The lumbar samples had lower stiffness (~-13%) and strength (~-17%) than the other samples (Table 1).

Differences after controlling for the density

After controlling for the major effect of density on mechanics, the differences between the 9 *subjects* were reduced (Figure 8 B and D) but remained significant for the stiffness ($p < 0.001$) and strength ($p < 0.001$). Subject to subject differences in stiffness and strength as high as ~40% were still observed (i.e. comparing subject C and D).

The introduction of the density for the prediction of stiffness and strength eliminated the level effect, meaning that differences in strength and stiffness between the levels were due to slight differences in

Table 1. Density and mechanical parameters according to the location variables (mean ± SE)

		Mechanical parameters estimated		Mechanical parameters for a density value of 0.175 g/cm^3	
	Density (g/cm^3)	Stiffness (MPa)	Strength (MPa)	Stiffness (MPa)	Strength (MPa)
Vertebral level					
T9	0.18 ± 0.01	366 ± 26	2.60 ± 0.20	332 ± 8	2.36 ± 0.07
T12 or L1	0.18 ± 0.01	366 ± 21	2.39 ± 0.15	365 ± 6	2.39 ± 0.05
L4	0.17 ± 0.01	344 ± 18	2.18 ± 0.13	350 ± 7	2.23 ± 0.06
Sample site					
Anterior	0.16 ± 0.01	334 ± 19	2.26 ± 0.14	361 ± 7	2.45 ± 0.06
Posterior	0.20 ± 0.01	434 ± 19	2.90 ± 0.15	386 ± 8	2.54 ± 0.06
External	0.16 ± 0.01	279 ± 18	1.75 ± 0.12	300 ± 9	1.99 ± 0.07

mean density. Regarding the *coring site* effect, the introduction of the density in the model explained the difference in stiffness and strength between the anterior and posterior samples, but external samples still had lower mechanical properties than the anterior (~18%) and lower than the posterior (~24%).

Discussion

Overall these observations strongly support the concept of bone quality. The relationship between density and mechanics varied significantly among subjects.

While the measurement of the strength of cancellous bone has never been a problem, the measurement of stiffness (the elastic modulus) is more demanding because accurate strain measurements are needed. However, in material mechanics, the modulus is a crucial parameter. We used a method for the compressive test of cancellous bone that was specially designed to measure accurately the structural stiffness of a cylindrical sample (Keaveny et al. 1997). The absolute values reported in this section are consistent with the data reported by those who designed the method (Kopperdahl and Keaveny 1998).

Simple correlation coefficient (r) between density and stiffness was 0.90 (figure 6 A). Hansson et al. (1987) found a r value of 0.85 using 231 vertebral cubic samples procured from 3 subjects. Mosekilde and Danielsen (1987) had correlation coefficient of 0.89 between strength and ash density using 40 vertebral samples from 40 patients.

The present investigation and those reported by the literature are consistent in showing that density does not account for, at least, 20% of the variance in stiffness and strength. Technically, this scattering can be due to random errors during the test or in measuring the density. It could also indicate that some samples had better bone quality than others.

The originality of our approach is to investigate whether systematic factors (subject or location of origin) can explain this scattering. Certainly the low mechanical properties of the external samples stand as an interesting enigma. This point should not be ignored for the design of future investigations.

To our knowledge, there has been no biomechanical study to support the concept of bone quality that was originally supported by the clinicians. For example, if we consider two male subjects (C and G) with the same mean density (0.16 g/cm^3), the former had a mean stiffness of 245 MPa and a strength of 1.54 MPa while the latter (that was older) had a mean stiffness of 347 MPa and a strength of 2.19 MPa. The data presented here demonstrate that, even when taking into account the differences in density, some subjects had higher strength and stiffness than others. Of course, different subjects had different densities, but when accounting for this parameter, the differences remained (as high as 40%, Figure 8 B and D).

So, while many authors suspected that bone quality varied among subjects or patients, we make the biomechanical demonstration of that fact.

Ultimately, if the vertebral cancellous bone samples from a subject behaves differently than those from another subject, it must be because they were physically different.

However, our original approach indicates new landmarks for the search of the factor(s) that may account for such differences in bone quality. If our final goal is to improve the prediction of the fracture risk for a patient, explaining the differences between subjects is much more relevant than understanding the differences due to the location of origin of the sample (Table 1) or due to unavoidable measurement errors.

When investigating various physical properties of the samples as potential indicators of the bone quality we will consider that it should:

a) vary significantly among subject and hence, be subject-specific. Indeed, those parameters that do not vary among subjects will never be able to explain the subject-specific differences in bone quality.
b) improve the prediction of the mechanical parameters after accounting for the density. Hence, the candidate must either be independent to density, or be normalized for the density.

Part II: Structural organization of the trabeculae

Introduction

Description of the cancellous bone

Bone volume fraction

The cancellous bone is a highly porous material. Typically in humans, 5 to 30% of its volume is hard bone tissue and the remaining part is soft tissue (bone marrow, vessels…). The fraction of the total volume occupied by bone tissue is called bone volume fraction (BV/TV) by morphologists. It is the morphological corollary of the density. Variations in density are closely correlated to variations in BV/TV ($r > 0.90$). Consequently, the BV/TV stands as the main predictor for the mechanical properties of the cancellous bone (see part I). Not only the BV/TV or density varies among patients, but it also changes from one anatomical location to another, within a given subject. In the vertebral body its value is especially low (<10%, Figure 9) while in the femoral head it is much higher (> 20%).

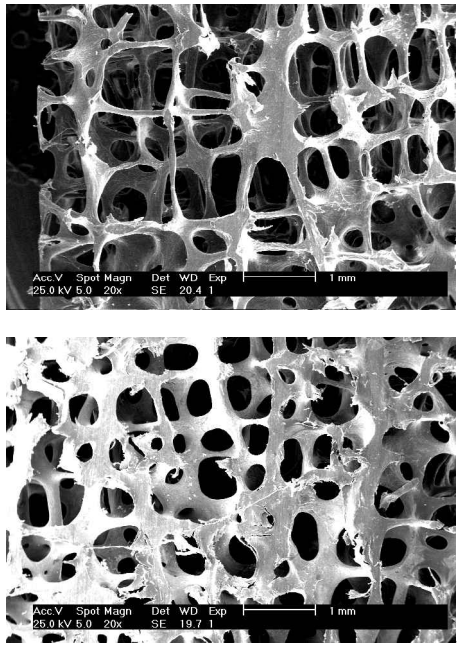

Figure 9. Vertebral cancellous bone as seen on scanning electron microscopy (or SEM). (A) One sample has low BV/TV (~4%). The other (B) has higher BV/TV (~10%).

A cellular material made of plates and rods

The overall structure of the cancellous bone has been compared to an 'open-celled' cellular foam (meaning that the cells or pores communicate with each other). The walls of each element are made up of trabeculae which can be idealized as plates (plate like elements) and rods (beam-like elements). Gibson et al. have individualized plate-plate structures, plate-rod structures and rod-rod structures (1985). Such description clearly illustrates how multiple cancellous bone architectures may coexist in the same patient. Each architectural 'design' reflects the local function of the tissue. In the vertebral body, the cancellous bone is best described as a rod-rod structure (Figure 9A) or a plate-rod structure (Figure 9B).

To grasp the potential importance of the micro-architecture only simple observations are needed. Consider a cube of cancellous bone from the proximal tibia. When tested in the vertical direction the mean modulus is 1100 MPa, in antero-posterior and in medio-lateral direction the modulus is 400 MPa (Ashman and Rho 1988). However, the density or BV/TV did not change since the same cube was tested. This example illustrates the *anisotropy* of cancellous bone (a mechanical concept). Note that for the human vertebral cancellous bone, the anisotropy is even more pronounced since the strength and stiffness are three times higher when bone is loaded in vertical direction (as we did in part I) than when loaded in horizontal direction (Mosekilde and Danielsen 1987). The mechanical anisotropy results from the structural anisotropy of the trabeculae. In many skeletal sites, they are oriented in a given direction (vertically in the vertebra) to support loading in a given direction.

'Connectivity' of the structural elements

In addition to their preferential loading axis, other aspects of the structural organization of the trabec-

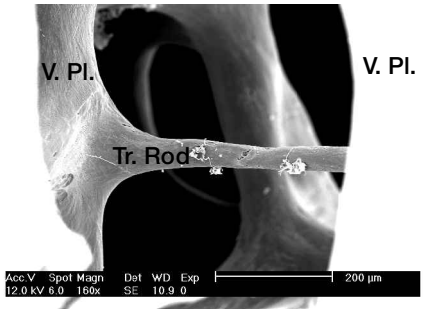

Figure 10. Strong vertical plates (V.PL) are linked or 'connected' by thin transverse rods (Tr. Rod). When the sample was loaded vertically the transverse rod prevents the bending and buckling of the vertical plates. A close-up view of the oblique fracture seen in its center was used as cover illustration.

ulae may influence their load bearing capacity.

In 1967, Bell et al. observed that age related decline in bone strength was much more pronounced than the decline in density (Bell et al. 1967), an observation confirmed by other studies (Mosekilde and Danielsen 1987; Weaver and Chalmers 1966). In Bell's original paper, A. Gibb, an engineer, gave a mechanical explanation to this observation using a simple model of vertical plates with interconnecting transverse rods. When loaded vertically the plates tend to buckle, a phenomenon that is prevented by the transverse rods. Such a simple model (vertical plates and horizontal transverse rods) is especially adapted for the vertebral cancellous bone, which is highly oriented (and thus, mechanically anisotropic). Short, well connected plates are theoretically much more efficient —mechanically—than disconnected plates. This concept is further supported by the observation of selective fracture on the transverse bars in a sample of vertebral cancellous bone tested in compression (Figure 10).

Efforts to quantify the structural organization

An enormous amount of work has been done to find descriptive parameters that would quantitatively measure the connectivity. This is an issue since, according to Parfitt (1983), the loss of structural connectivity is an irreversible process as new lamellar bone can only be added on an existing surface. These authors described parameters derived from the perimeter and surface measurements (Trabecular thickness, Tb.Th; number Tb.N, and spacing, Tb.Sp). Others quantified the number of connections (Nodes, Nd) and disconnections (Free-ends, Fe) form the trabecular network (Compston 1994); or the relative amount of concave and convex surface (Trabecular bone pattern factor, TBPf) (Hahn et al. 1992); or the chord distribution in the marrow space (Star volume) (Vesterby 1990). Additionally, while all of these parameters have been described on two-dimensional images, the recent development of 3D acquisition tools has led to the description of many 3D architectural parameters. Overall, about 100 of such parameters could be referenced, every team having its own, preferred set of parameters…

Nowadays, the microarchitecture is included in the definition of osteoporosis (see part I). This underlies two ideas. First, with aging or osteoporosis, there is a deterioration of microarchitecture (in addition to the reduction of density). Second, microarchitecture should improve the prediction of bone mechanical properties. Analyzing the data from the literature, things are not as obvious as they appeared.

Iliac crest biopsy

Multiple studies have underlined the usefulness of iliac crest biopsy as a tool to investigate the integrity of the trabecular network. Most studies have reported that the connectivity was significantly lower in the patients suffering from vertebral crush fractures when compared to density matched controls (with either iliac BV/TV or vertebral BMD). Referring to the introduction of part I, the goal of these studies is to reduce the 'overlap' between fracture and non-fracture groups using the microarchitecture of the iliac crest biopsy. A low Tb.N in the iliac crest biopsy has been presented as a good predictor of vertebral fracture risk in postmenopausal women (Kleerekoper et al. 1985); this information has been confirmed (Recker 1993; Kimmel et al. 1990) or not confirmed (Oleksik et al. 2000) by others. Some studies showed that the strut analysis or star volume would be more efficient (Recker 1993). In men osteoporosis, the Tb.N was also decreased while index of connectivity derived from the strut analysis of the medullary cavities (ICI) was also altered (Legrand et al. 2000). Overall, the literature is somewhat consistent. The addition of iliac crest microarchitectural parameters to bone mass (either BMD or BV/TV) improves the

ability to differentiate between patients with and without fractures.

However, several points should be borne in mind when considering these data. First, no prospective study demonstrated the capacity to announce the fracture before its occurrence. Changes in iliac crest morphometry could happen consecutively to fracture (Heaney 1992). Further, the fracture and microarchitecture were assessed in different skeletal sites. The correlation between iliac crest parameters and lumbar vertebra is 0.7 (r value) at best for strut analysis (Mellish et al. 1991) and has been reported not significant for the Tb.Th (Alexiades et al. 1990). Finally all parameters are certainly operator dependent, and there is no consensus regarding which one is the key parameter.

Moving to specific sites

Nowadays, clinical tools—i.e. CT scans (Gordon et al. 1998) or MRI (Majumdar et al. 1998) for the spine and pQCT or MRI for the wrist (Gordon et al. 1996)—seem to give some access to the trabecular bone morphology, within an anatomical site that is most prone to fracture. Contrary to the morphometrical assessment of the iliac crest biopsy, there is no discrepancy between the site of measurement and the site for which fracture risk is estimated.

Microarchitecture and bone strength: in vitro studies

All the above mentioned investigations are based on the idea that connectivity influences the mechanical behavior of bone. However, to date, there is no solid demonstration of such a relationship. Some studies using powerful µCT scan, 3D reconstruction and finite element analysis (FEA) to simulate the mechanical behavior have enhanced the importance of 3D microarchitectural parameters (Kabel et al. 1999; Ulrich et al. 1999; Kabel et al. 1999; Van Rietbergen et al. 1998). In these investigations, the samples were not actually tested, and the study remained completely virtual. FEA calculation requires hours of computing time per sample on powerful workstations. Even considering the simulated mechanical properties as reliable, these studies do not deliver a consistent message.

In testing iliac crest samples, Thomsen et al. (1998) tried to improve their prediction of strength using multiple connectivity indices. They concluded that none of them could improve the prediction obtained with the single BV/TV value. For the vertebral cancellous bone no study has compared histology and mechanical tests. Using the pQCT as a morphological investigation tool, Jiang et al. (1998) tested 26 vertebral cubes (12 x 12 x 12 mm) from 7 subjects and report that the addition of Nd *and* Fe to BMD modestly improved the prediction of bone strength (r^2 raised from 0.76 with BMD alone to 0.86 with 3 predictors). Majumdar et al. (1998), probably using the same set of samples, investigated microarchitecture with high resolution MRI. They used QCT to measure the BMD and obtained an unusually low correlation coefficient between BMD and strength ($r^2 = 0.50$). The addition of the Euler number (an indicator of connectivity extracted from the MRI images) to the BMD improved the prediction of the strength to $r^2 = 0.65$.

In 1994, J. E. Compston said that 'The concept that connectivity is a major determinant of bone strength may require revision.' (Compston 1994). She was hoping that new technologies—i.e. µCT scans, and 3D assessment of bone structure—would provide new insight into structural and mechanical consequences of bone loss.

As far as we know, two large studies have combined mechanical and µCT assessment of cancellous bone: Ding et al. on the tibial plateau (Ding 2000) and the BIOMED I study on multiple skeletal sites (Dequeker 1994). Despite of a wide sampling (> 30 subjects included, age range 20–90, hundreds of sample tested) and an extraordinary access to the microarchitectural data (Day et al. 2000; Hildebrand et al. 1999), none of these studies resulted in the publication of a significant improvement of the prediction of bone strength using 2D or 3D architectural parameters.

Overall, the link between structural organization of the trabeculae and bone strength still stands as concept rather than a fact.

Working hypothesis

In Part I we demonstrated that bone quality is a biomechanical reality. In this section, we investigate whether microarchitecture accounts for the differences in bone quality.

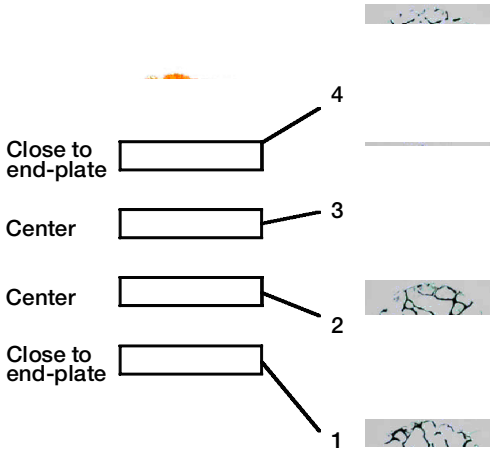

Figure 11. Four transverse thin sections were obtained in each sample; two from the center of the core (2 and 3) and two from a region 'close to end-plate' (1 and 4).

Consequently we explored the following hypotheses:

a) The microarchitecture of the vertebral cancellous bone is patient specific. In other words, the microarchitecture itself (apart from the density) allows us to distinguish a subject from another.
b) The structural parameters improve the prediction of bone mechanical properties (stiffness and strength).

Materials and methods

The cohort of 136 cylindrical samples used in part I was split in two groups. Cores from one side were used for the histological assessment while those from the contralateral side were used for the biochemical analysis (see part III).

Histomorphometry

The 68 samples dedicated to histology were fixed, and embedded in Spurr resin using a standard protocol (Schenk et al. 1984). The plastic blocks containing the whole cylindrical specimens were then cut at four levels to cover its volume from bottom to top (Figure 11). This was done using an Exact® cutting grinding machine. The small blocks were re-embedded to allow a correct fixation in the microtome (Jung Polycut). After trimming to expose the bone, 5 μm sections were cut. One was deplasticized and stained with Von Kossa which visualizes the mineral in black.

The stained slices were then placed on a luminescent table and photographed using a Tessovar stereomicroscope (Carl Zeiss, Oberkochen/Württ, Germany) on which a digital camera was mounted (Banse et al. 2002). A single picture (2048 × 1536 pixel) covering the whole slice image was obtained. All 272 pictures were taken with the same settings, based on the most appropriate contrast and resolution. These images were then downloaded on a computer, cropped to fit the edges of the cylinder and resized to a standard size of 768 × 768 pixels (using Adobe Photoshop® 5.5). Pixel size was 10.67 μm (Figure 13).

Image analysis was performed with a Quantimet 500 IW using Qwin Pro (Leica Imaging System, Cambridge, UK). The images were converted to binary images using a 'darker than 100' threshold. The classical morphological parameters were measured according to the ASBMR nomenclature (Parfitt et al. 1987) on these binary images. These included the trabecular volume fraction (BV/TV, %), the trabecular number (Tb.N, mm^{-2}), the trabecular thickness (Tb.Th, μm) and the trabecular spacing (Tb.Sp, μm). The binary images were then skeletonized and pruned to quantify the total strut lengths (TSL, mm/mm^2). Pruning procedure consisted in elimination of parasiting branches with a size inferior to the Tb.Th. The multiple points or nodes (Nd, mm^{-2}) as well as the free-ends (Fe, mm^{-2}) were then identified on this skeleton (Compston et al. 1987). The ratio of the number of nodes and number of free-ends (Nd/Fe, -) was also calculated and considered as an index of connectivity. Finally, we measured the star marrow space (Star, mm^2) (Gordon et al. 1998; Vesterby 1990). For this parameter, a seed is grown within the marrow in multiple directions until intersecting a trabecular bone. The surface area of the star created is then calculated. A total of 9 structural parameters were obtained.

Data processing and statistical analysis

First, the link between the BV/TV and the other parameters was investigated using simple correlations. As most of the morphometrical parameters

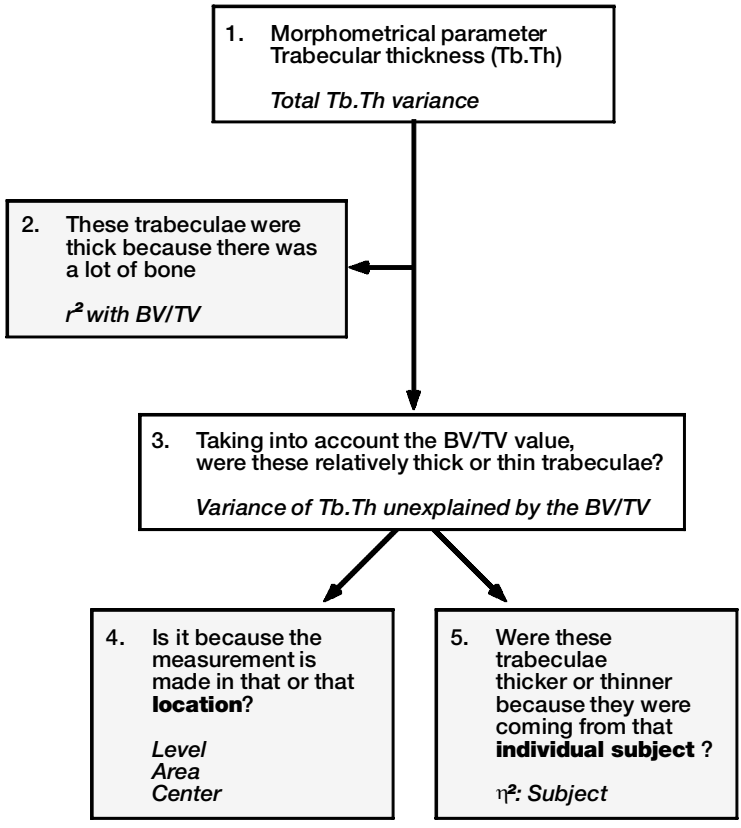

Figure 12. Flow chart showing how the morphometrical data were analyzed. For detail, see text.

depended on the BV/TV (see Table 2) we were concerned by their ability to *add information* to the density or BV/TV measurement. We postulated that, after being weighed for the BV/TV, the morphometrical parameter should still be able to enhance structural differences between various anatomical sites (intra-individual or within-subject differences) or differences between the nine subjects (inter-individual or between-subject differences).

We used the same statistical approach as in part I. The morphometrical parameters (either Tb.Th, Tb.N, Tb.Sp, TSL, Nd, Fe, Nd/Fe, Star) were the dependent variables (Figure 12, box 1). The BV/TV was introduced first as a covariable (Figure 12, box 2), meaning that the observed variance was reduced to the 'added-information' we wanted to explore (Figure 12, box 3). The location variables (vertebral *level* and the *coring site*) within the vertebra were considered as having a fixed effect. Additionally, images coming from slices 1 and 4 were computed as coming from the *close-to-end-plate* slices and slices 2 and 3 from the *center* slices. Whether the measurement was obtained from the center or not was the third location variable (Figure 12, box 4). The name of the *subject* was introduced as having a random effect (Figure 12, box 5). To compare the capacity of the various morphometrical parameters to enhance differences between subjects we obtained the Eta-squared (η^2) value from the mixed model. η^2 is an estimate of the portion of the total variability explained by the variations in the independent variable (here the *subject*). As in Part I, an estimated marginal mean representative of a given subject was calculated from the model and used for chart presentation of the results.

The relationship between mechanical properties and morphological parameters was explored using a stepwise multiple regression model. Such a model was used to determine the combined effect of BV/TV and architectural parameter on the prediction of the stiffness and strength of the samples (for measurement see Part I). The partial correlation coefficients (r) for the morphometrical parameters were reported.

Results

General observations

Our data confirm the low density of the samples, only 8% of the volume being occupied by bone. The trabeculae were thin (84 μm) and widely spaced (> 1000 μm). The nodes (Nd) were relatively rare, with less than 1 node/mm² and about three free-ends (Fe, or disconnection) for a node.

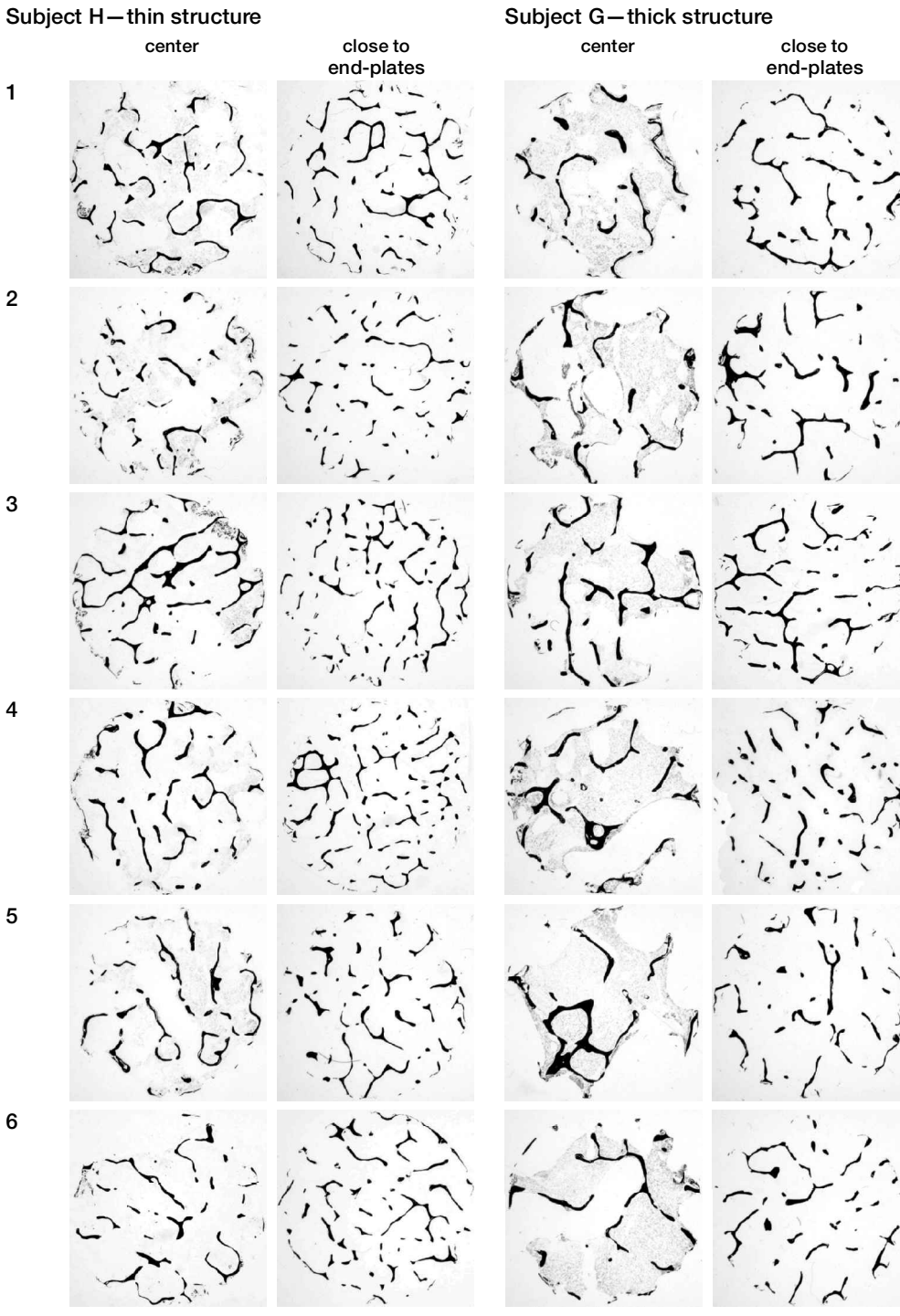

Figure 13. Thin sections (5μ) of the vertebral cancellous bone enhancing two different structural organizations of the trabeculae.12 slices (Von Kossa staining, the width of a square image is 8.2mm) from identical anatomical locations but from two different subjects (H, left and G, right) are compared. In one column, slices come from the center of the vertebral body and in the other column they come from closer to the end-plate. Each row corresponds to a given cylinder: 1, 2 and 3 were respectively the anterior, external and posterior cylinders from the thoraco-lumbar (L1) vertebra and 4, 5 and 6 were respectively the anterior, posterior and external cylinders from the lumbar (L4) vertebra. (Modified from Banse et al. 2002c, with permission)

Table 2. Microarchitectural parameters (n = 68)

Parameter	Mean	SD	Corr. with BV / TV (r)
Amount of bone			
BV / TV (%)	7.9	2.3	
Structural parameter			
Tb.Th (µm)	84	13	0.76 [b]
Tb.N (–/mm^2)	0.93	0.18	0.86 [b]
Tb.Sp (µm)	1050	231	-0.83 [b]
TSL (mm/mm^2)	0.78	0.17	0.85 [b]
Nd (–/mm^2)	0.81	0.24	0.85 [b]
Fe (–/mm^2)	2.49	0.43	0.16
Nd / Fe (–)	0.33	0.08	0.87 [b]
Star (mm^2)	6.9	2.2	-0.80 [b]

Mean and standard deviation of the morphometrical parameters. The link or correlation between the BV/TV and the other morphometrical parameters is estimated (r = simple correlation coefficient).
Key: [a] $p < 0.05$, [b] $p < 0.001$

All these raw parameters (except the Fe) were highly correlated to the BV/TV (Table 2).

Differences between subject and locations

Variations in BV/TV directly follow the variations in density, which are detailed in part I (r between BV/TV and density = 0.94). After controlling the major effect of BV/TV, all structural parameters were clearly patient specific (Figure 14). Enhancing differences between patients was easier using some parameters than using others. The most efficient parameters were the Tb.Th and Fe ($\eta^2 > 0.70$, $p < 0.001$), then Tb.N, Tb.Sp, TSL, Star and Nd ($\eta^2 > 0.45$, $p < 0.001$). The Nd/Fe had the lowest capacity to differentiate the subjects ($\eta^2 = 0.34$, $p < 0.05$). The maximal differences observed between two subjects was ~30% for most parameters but ~50 % for the Star and Fe.

The structural organization of the trabeculae was also found to be slightly different according to the anatomical location (Table 3). In the L4, the trabeculae were found to be slightly thicker (Tb.Th), less numerous (Tb.N), more spaced (Tb.Sp) and spreading over a shorter network (TSL) than at the T9 or T12-L1 vertebral levels but the differences were small (5–10%). No major differences were noted between the coring sites although, after correction for the BV/TV, the model noted 12–14% more Fe in the posterior samples and consecutively a lower connectivity (Nd/Fe ~10%, Star ~8%).

Comparing the central part of the vertebra and the close to end-plate regions, all the structural parameters varied. The central trabeculae were clearly thicker (9%), less numerous (7%) and more spaced (8%) than those located closer to the end plates. Further, less nodes (11%) and much less free-ends were observed in the center (25%). Consistently, the Nd/Fe and Star were higher in the center than in the close to end-plate regions (15%

Table 3. Microarchitectural parameters according to the location variables evaluated for a BV/TV = 7.9% (Estimated Marginal Mean ± SE)

	Tb.Th T(µm)	Tb.N (–/mm^2)	Tb.Sp (µm)	TSL (mm/mm^2)	Nd (–/mm^2)	Fe (–/mm^2)	Nd / Fe (–)	Star (mm^2)
Vertebral level								
T9	82.7 ± 1.1	0.95 ± 0.01	1029 ± 20	0.80 ± 0.01	0.80 ± 0.02	2.49 ± 0.06	0.32 ± 0.01	6.7 ± 0.2
T12 or L1	81.1 ± 0.8	0.96 ± 0.01	1022 ± 16	0.81 ± 0.01	0.85 ± 0.02	2.54 ± 0.04	0.34 ± 0.01	6.7 ± 0.2
L4	86.4 ± 1.0	0.89 ± 0.01	1097 ± 18	0.75 ± 0.01	0.80 ± 0.02	2.48 ± 0.05	0.34 ± 0.01	7.5 ± 0.2
Sample site								
Anterior	84.3 ± 0.9	0.92 ± 0.01	1056 ± 17	0.78 ± 0.01	0.79 ± 0.02	2.36 ± 0.05	0.35 ± 0.01	7.0 ± 0.2
Posterior	81.5 ± 1.0	0.96 ± 0.01	1019 ± 19	0.79 ± 0.01	0.84 ± 0.02	2.72 ± 0.05	0.31 ± 0.01	6.5 ± 0.2
External	84.5 ± 1.2	0.92 ± 0.02	1073 ± 23	0.78 ± 0.02	0.82 ± 0.03	2.43 ± 0.06	0.34 ± 0.01	7.3 ± 0.3
Center								
Center	86.8 ± 0.6	0.90 ± 0.01	1086 ± 11	0.76 ± 0.01	0.77 ± 0.02	2.20 ± 0.04	0.36 ± 0.01	7.4 ± 0.1
End-plate	79.7 ± 0.6	0.97 ± 0.01	1010 ± 11	0.81 ± 0.01	0.86 ± 0.02	2.81 ± 0.04	0.31 ± 0.01	6.5 ± 0.1

Result of the mixed model for the microarchitectural parameters. The estimated marginal means are adjusted for a BV/TV value of 7.9 % (the overall mean). In the lumbar vertebrae the trabeculae were slightly thicker and more spaced. All microarchitectural parameters were different in the center of the vertebral body, when compared to the close to end-plates region.

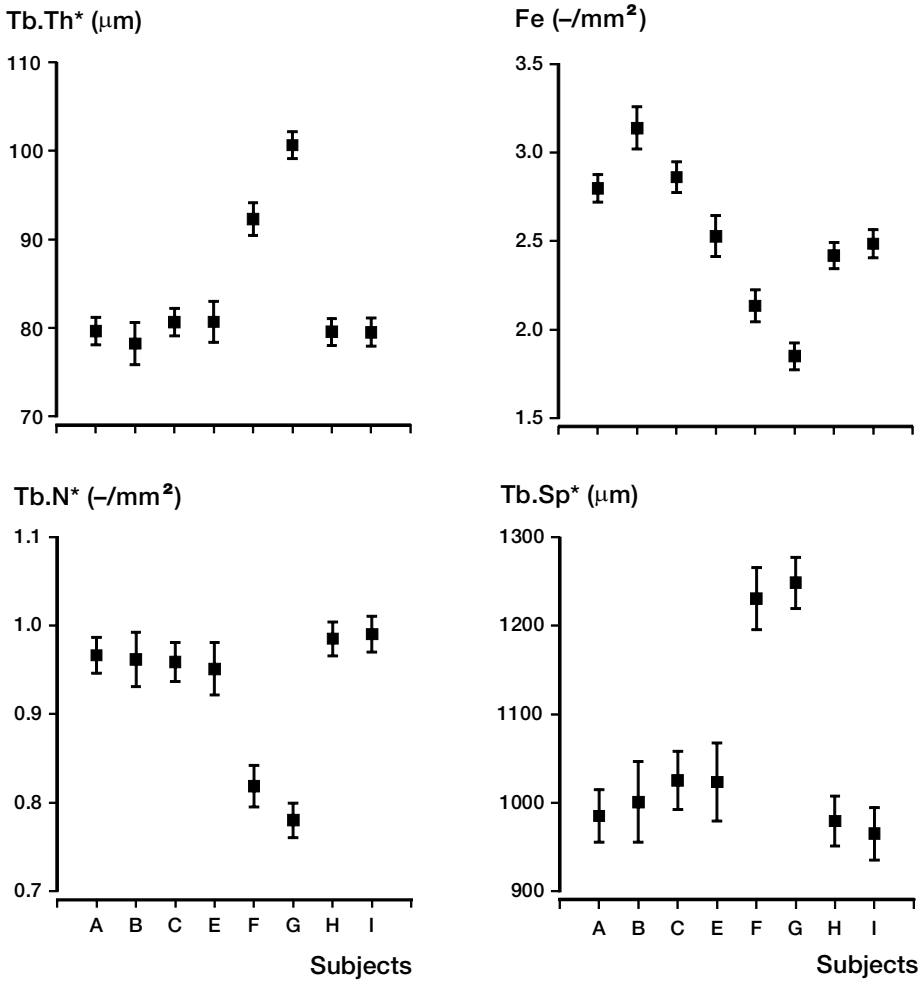

Figure 14. Variation of the morphometrical parameters among subjects. When indicated (*) the morphometrical parameter was normalized according to the BV/TV. The square indicates the mean value and the bar the standard error. The order of appearance of the charts reflects the capacity of the parameters to differentiate the subjects. Measuring the Tb.Th or the number of Fe (in addition to the BV/TV) allowed to distinguish the subject easily (small error bars) while this was more difficult using the Nd or Nd/Fe data. (Modified from Banse et al. 2002b, with permission from Elsevier Science).

and 13% respectively). Note the contradiction since one indicates higher connectivity and the other lower connectivity in the center. All of these differences were significant ($p < 0.001$).

Correlation with the stiffness and strength

The correlation between stiffness or strength and BV/TV was excellent (Table 4). Consecutively, the BV/TV always came out as first predictor of strength and stiffness in the stepwise regression procedure. No histological parameter could improve the prediction of the stiffness, except the Star (when included, the adjusted r^2 changes from 0.79 to 0.80, $p < 0.05$). For the prediction of the strength the addition of the Tb.N, Tb.Sp (r^2 changes from 0.76 to 0.78, $p < 0.05$), as well as the star (r^2 changes from 0.76 to 0.79, $p < 0.05$) slightly improved the prediction.

Discussion

This part of the study indicates that the structural organization of the vertebral cancellous bone was clearly a patient specific parameter. Additionally, systematic anatomical patterns have been identified, mainly in the center of the vertebral body.

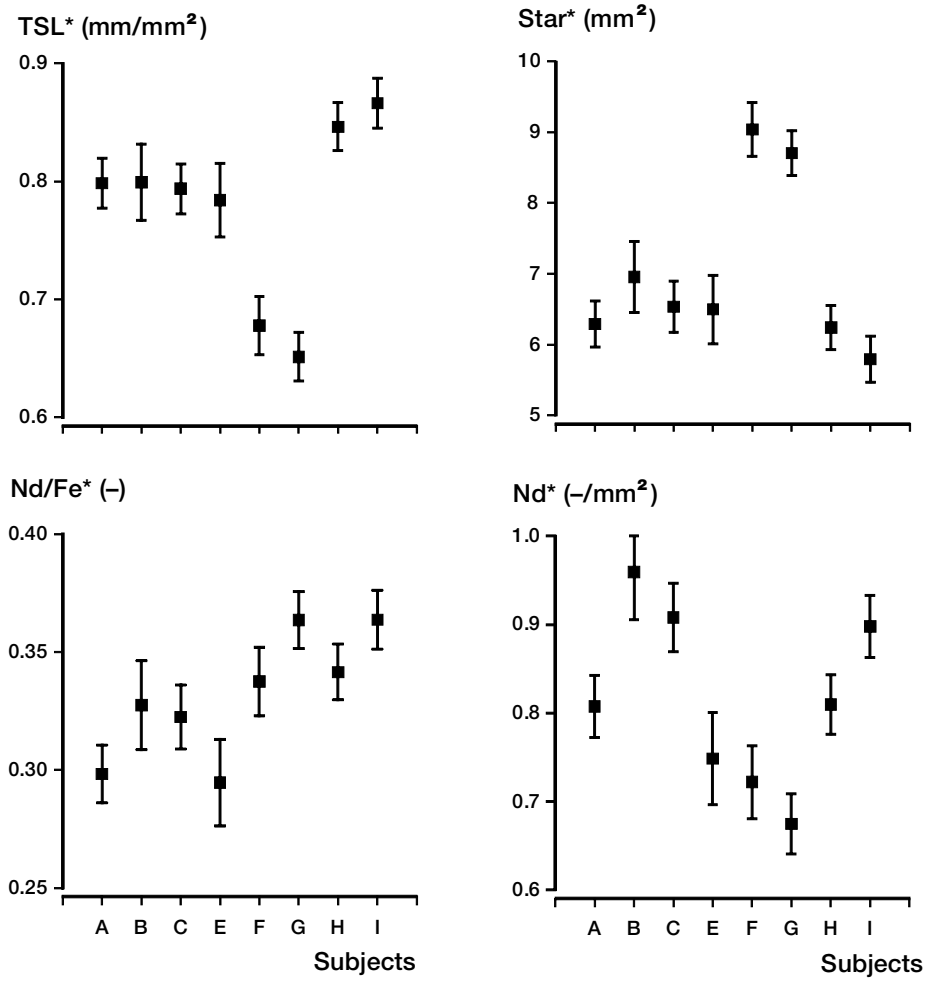

Figure 14. Continued.

The contribution of bone architecture to bone strength is overruled by the bone volume fraction and only marginal improvements in the prediction of the mechanical properties have been noted.

Amount and structural organization of trabecular bone

The link between the amount of bone (BV/TV) in a section and its organization (as described by the morphometrical parameters) is very tight, especially when focusing on a single anatomical region like the vertebral body (Jiang et al. 1998; Gordon et al. 1998; Snyder et al. 1993). The correlation we found between BV/TV and the other parameters are consistent with the other data published data. Compston et al. (1989) observed a good correlation between BV/TV and Tb.Th ($r^2 = 0.61$) in iliac crest biopsies but also found a weaker relationship between the BV/TV and the Fe ($r^2 = 0.23$). Chappard et al. (1999) have also shown comparable relationships between the BV/TV and various architectural parameters.

In our data high BV/TV was associated with high Tb.Th, Tb.N, TSL, Nd, Nd/Fe and low Star or low Tb.Sp (Table 2). Additionally, most structural parameters were inter-correlated, even when measured with different methods, i.e.–the TSL and Star (Figure 15). This has been noted and commented on by others (Chappard et al. 1999; Croucher et al. 1996). At some point, these correlations indicate a consistent organization in a structure that looks disorganized.

Table 4. Correlation between microarchtitectural parameters and mechanical parameters

Parameter	Stiffness (MPa)	Strength (MPa)
Amount of bone		
BV / TV (%)	0.89 [c]	0.88 [c]
Structural parameter		
Tb.Th* (µm)	-0.13	-0.24
Tb.N* (–/mm^2)	0.21	0.31 [a]
Tb.Sp* (µm)	-0.21	-0.33 [b]
TSL* (mm/mm^2)	0.15	0.24
Nd* (–/mm^2)	-0.01	-0.05
Fe (–/mm^2)	0.12	0.12
Nd/Fe*(–)	-0.12	-0.20
Star* (mm^2)	-0.28 [a]	-0.37 [b]

For the BV/TV, the simple correlation coefficient is given. For the other microarchtitectural parameters, the table presents the partial correlation coefficient (r) after controlling the major effect of the BV/TV (for instance, as a second predictor).
Key: [a] $p < 0.05$, [b] $p < 0.01$, [c] $p < 0.001$

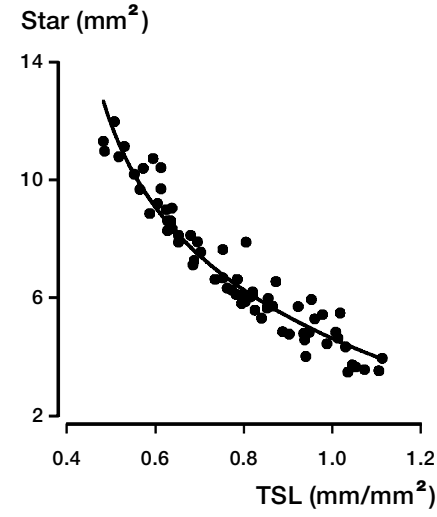

Figure 15. Correlation between the TSL and Star. Both parameters are measured using totally different techniques.

Fortunately the link between BV/TV and the other parameters was not perfect. Should the correlation coefficient be 1, it would be useless to assess the morphometry, and only the BV/TV or density would describe the whole structure. If the link is not perfect, we need to know if the variability that was not explained by the BV/TV just happened at random or whether it can be a location / subject dependant parameter (Figure 12).

This is the reason for the initial introduction of the BV/TV in the mixed model. As many reliable and reproducible techniques allow a correct measurement of the patient's apparent density (DXA, QCT…), our rationale was that only the 'extra-information' or purely structural information contained in the morphometrical parameters was worth being analyzed.

The structural organization is patient-specific

The final goal of histomorphometry is to enable the investigator to detect patients that have a significantly different trabecular organization. In this study, we demonstrate that morphometrical parameters add some patient specific architectural information. Technically, to enhance such architectural differences between one subject and another, multiple measurements are required. Conclusion cannot be drawn from a single measurement for each subject. With a single value it is impossible to know whether the variability of the value is due to random error or to a subject specific pattern.

A systematic analysis of the morphometrical parameters allowed us to pick up those that had the best ability to differentiate patients. It seems clear that Fe and Tb.Th were the most sensitive parameters, although most of the structural characteristics varied among patients. On the thin sections, differences may not be obvious if the BV/TV is not equal. However, when the density or BV/TV was the same, as for the subjects G and H (~0.16 g/cm^3, ~7.7 %, Figure 13), the difference in structural organization was obvious, and the quantification of structural parameters just come to support the conclusion of a gross examination of the thin sections. Comparing patients G and H, there was a ~20% difference in Tb.Th, Tb.N and TSL and a ~30% difference in the Fe or Star.

Certainly, the structural parameters meet the first condition to be indicators of bone quality (they vary significantly among subjects).

Architecture in the center of the vertebrae

In 1543 the anatomist Andreas Vesalius of Brussels noted that "The larger and the more imposing the body of a vertebra, the less solid and the more fun-

gous it is and the more varied and unequal holes in it". He had observed the substance of the vertebral body (the cancellous bone) and had correlated the microarchitecture to the vertebral level. Vesalius also describes how the aspect of the bone could be related to the vessels and offshoots of the veins that enter the vertebral body through the posterior face and in its middle portion. Using sophisticated modern methods our data simply confirm the observations of Vesalius. For instance, the Star in the center of the vertebral bodies was 6.3 mm at T9 level, 7.1 mm at T12–L1 level and 7.9 mm at L4 level (great!). Note that, if big 'pores' were observed in the center of the vertebral body, it does not mean lower density of BV/TV; simply the architecture is different, not the amount of material. Beside the penetration of the vessels, the growth of the vertebral body may be responsible for the central structure pattern. The ossification of the vertebral body begins in the center of the body, progressively reaching the endplates…

Practically, the structural difference between the center and the close to end-plate regions had some implications. Each of our cylinder was actually composed of a stack of segments with thinner and thicker (center) structures. Most probably, a limited segment of the cylindrical column failed. We do not know in which segment the failure occured.

Structural organization and bone strength

The addition of the morphometrical data resulted in only marginal improvements (1 to 3%) of the prediction of strength and stiffness. We did not find the morphometry as having a dominant effect on cancellous bone mechanics. We agree with the skepticism of J.E. Compston (see introduction). The contribution of microarchitecture to bone strength appeared as marginal and was certainly *not sufficient* to account for the substantial differences in bone quality that we observed between subjects (as great as 40%, see part I). None of the architectural parameters could account for such differences. However, maybe the samples with high Star surface and low Tb.N had slightly lower properties.

In a recent work Gordon et al. (1998) studied the in-vivo architecture of the vertebral cancellous bone, using high-resolution CT images. They improved their capacity to differentiate fracture and non-fracture patients using the BMD and one architectural parameter. They measured the same set of parameters as we did, but the star (they call H_A, hole area) stood as the best parameter to discriminate the fractured and non-fractured patients. In pointing out the Star, our data are consistent with this clinical study. However, we just included samples coming from 'normal subjects', with no obvious bone pathology (including no evidence of osteoporotic fractures). The osteoporosis may affect bone architecture with a magnitude that has not been captured by this study. Ideally, future in-vitro studies—combining biomechanics and microarchitecture—should include vertebral samples from osteoporotic patients to precisely assess that issue.

A point which is certainly demonstrated in our study is that different subjects with obviously different architecture—i.e. subjects G and H—may have the same mechanical behavior. Referring to Figures 8A and 8C in Part I, those two subjects did have the same strength and stiffness even after adjusting for small differences in BV/TV or density.

As we mentioned earlier, the ultimate method to account for the trabecular architecture is FEA. It is used in mechanical engineering to simulate the behavior of a complex structure. In a recent study, Hou et al. (1998) extracted 28 vertebral cancellous bone samples, used a μCT for assessment of the microarchitecture and tested the specimens in compression. FEA models were generated directly from the μCT images and compression was simulated. They obtained a good correlation between the actual testing and the simulation ($r^2 = 0.89$). However when trying to fit the 3D FEA model (that takes into account all the morphometrical information and the BV/TV) with the actual testing they calculated that the stiffness of the bone material was ranging from 2.7 to 9.1 GPa. As if some were made of relatively soft tissue and some of hard tissue. They could not relate that value to sex, age, race, weight or morphometry.

Limitations

The correlations

The use of multiple regression procedure using each sample as an independent data could be criticized, but it is the most straightforward, easy to interpret and frequently used in the literature

(Kabel et al. 1999; Jiang et al. 1998; Majumdar et al. 1998; Goulet et al. 1994). While the main issue remains the repeated nature of the data, such correlation tables must be considered as an effective screening tool.

Narrow window

At a given anatomical site, the bone architecture is adapted to its function, and consequently the link between stiffness and density. We found the BV/TV as well as the density, to explain ~80% of the variance in strength and stiffness. This means that the quest of new predictors for mechanical properties is done within a very narrow window that can be estimated as 20% of the variance. These 20% include unavoidable random errors in the mechanical testing and in the assessment of architecture. For instance, the size of the samples (8.2 mm in diam.) certainly resulted in random disruption of the trabeculae (during the extraction) that—randomly—affect the mechanical outcome. As one can see, the multiplication of parameters involved —i.e. stiffness plus BV/TV plus Tb.Th, results in an accumulation of random errors that blur the regression.

Static or dynamic properties

Our biomechanical testing only explored one aspect of the cancellous bone mechanical properties. The test was quasi-static (compression at low speed ~1mm/min). Neither shock, nor fatigue or creep were investigated. It may turn out that some architectures are more sensitive to one of these types of loading conditions, but not in quasi-static conditions that we used. Parameters like fracture toughness or work to failure were not considered. Furthermore, when crush fracture happens in osteoporotic patients it may result from a combination of compression, bending and shear while we just explored the compression.

Overall, our biomechanical parameters (stiffness and strength), although considered as key parameters in bone mechanic (Currey 1984), poorly simulate the events happening in vivo and leading to the structural failure of the vertebral body.

Finally, different structures,—i.e., where thin elements dominate, may be much more sensitive to the acceleration of the bone turn-over occurring after the menopause or in disease.

Conclusion of part I and II

If we concluded in part I that density did not fully predict bone strength, we can conclude form part II and from the currently published data, that both density *and* microarchitecture fail to precisely predict bone strength.

Part III: Properties of the organic matrix

Introduction

In a recent editorial, A. Boskey et al. (1999) wrote: "The relative amounts and properties of the mineral (apatite) and organic matrix (mainly type I collagen) in bone, as well as the organization of the bone at the microscopic and macroscopic scale (microstructure and anatomy, respectively), determine its mechanical strength'. In other words, the mechanical properties depend on three major parameters: the *amount* of bone material present (bone volume fraction or BV/TV, %), its *structure* (how it is distributed, organized and inter-connected in three dimensions), and its *nature* (chemical composition and organization of the bone matrix).

In part I and II, we have explored the influence of the amount and structure of bone material. In this introduction, we will give a general description of the nature of bone tissue, and a detailed description of the bone collagen. Then, we will analyze the collagen properties among patients and its potential influence on mechanics. Part III explores some aspects of the biophysical nature of bone tissue.

Looking inside a trabecula: bone tissue

In this part we will refer as bone tissue to designate the material that composes the trabeculae. In biological terms, the *extracellular matrix* of any tissue is most simply described as the material between the cells. While there are almost no vessels in trabecular bone tissue, numerous bone cells (osteocytes) are found in small lacunae surrounded by this extracellular matrix. The matrix is also permeated by tiny canals (canaliculi) containing cell processes, many of which interconnect in a syncytial network. These elements account for only 5% of the volume of tissue (Triffitt 1980).

Bone is a highly specialized connective tissue, obviously different from most other connective tissues by its content of calcium phosphate mineral. It can be seen as a dense packing of collagen fibers (the organic matrix, 25% of the dry weight), in which large amounts of solid mineral crystals are found (the mineral phase, 70% of the dry weight).

Using engineering terminology, bone tissue stands as a complex composite material. Increasingly powerful investigation tools (in microscopy, biochemistry, spectroscopy….) just increase the feeling of high complexity and heterogeneity in the material.

Sequences in the matrix deposition

The adult skeleton is in a dynamic state, being continuously broken down and reformed by the coordinated action of osteoclasts and osteoblasts on the surface of the trabeculae. Our current understanding of this 'bone remodeling' or turnover is based on the morphologic observation of Frost (1964), who observed that bone formation occurred almost exclusively at sites that had undergone resorption (Figure 16). The function of remodeling is to maintain the biomechanical competence of the skeleton by preventing the accumulation of fatigue damage and providing adequate supply of young bone (Martin and Burr 1982).

First, few *osteoclasts* (large, multinucleated cells) are activated and remove a packet of bone. They work fast, over 10 days. The resorption cavity (also called *Howship's lacuna*) is then filled by a team of osteoblasts which are attracted to the site and then proceed to make new bone. New bone deposition lasts for 3 months. First the osteoblasts synthesize the thin (6 µm) layer of organic matrix –or *osteoid bone*. The osteoid layer can be seen as a narrow zone of non-mineralized extracellular material between the osteoblasts and the underlying mineralized bone. Few cells leave the team and get embedded within the recently formed matrix, forming the osteocytes. After formation of a given layer of osteoid bone the organic matrix of the osteoid layer undergoes *maturation* during ~10 days (stabilization of the fibers by intermolecular cross-linking, see later). The precise organization of the organic matrix, as well as definite local conditions, induce the mineral deposit (Knott and Bailey 1998). The *mineralization* progresses from the

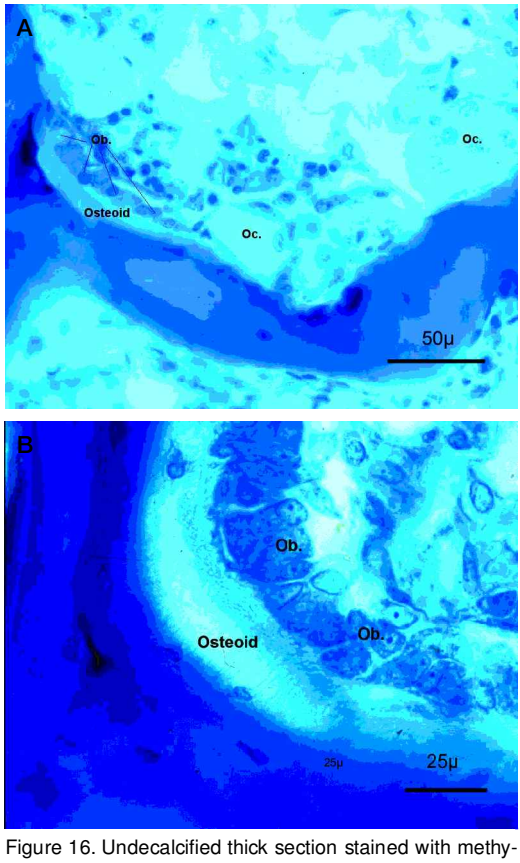

Figure 16. Undecalcified thick section stained with methylene blue showing a bone remodeling unit. A: Two osteoclasts (Oc.) are resorbing bone close to a site of active bone apposition. B: New bone matrix (unmineralized, osteoid) is deposited by a team of osteoblasts (Ob.). Courtesy of C. Behets-Nyssen, Dept. of Anatomy, UCL.

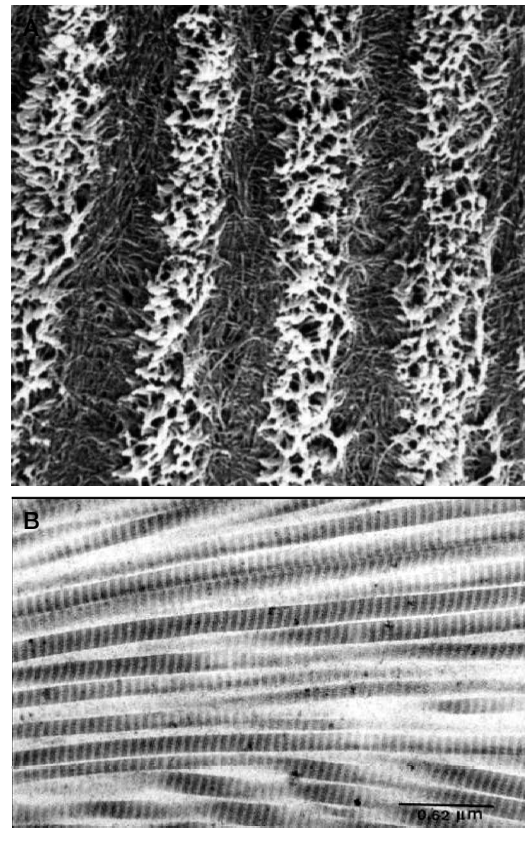

Figure 17. A: The major component of bone matrix is type I collagen. When a section of bone is superficially decalcified and examined with SEM (x 2000), abundant collagen fibers are seen, as well as the dense and loose zone of lamellation (Courtesy of G.Marotti, with permission). B: The typical striation of the collagen fibrils is best seen on TEM (Courtesy of J.F. Denef, Histology, UCL).

cement line to the osteoblasts while they go on forming another layer of osteoid. Each layer constitutes a highly organized *lamellae* (Parfitt 1988). Using electron microscopy, G. Marotti (1993) elegantly demonstrated that the lamella was made up of alternating collagen-rich (dense lamellae) and collagen-poor (loose lamellae) layers, all having an interwoven arrangement of fibers.

The organic matrix

Type I collagen is the principal constituent of the organic matrix (Figure 17A), representing 90% of its weight (Glimcher and Krane 1968). The cancellous bone also contents barely detectable amounts of type III and type V. These are primarily associated with bone vessels and osteocytes (Bailey et al. 1999).

Numerous noncollagenous proteins (proteoglycans and glycoproteins) have been identified in the bone matrix (Robey and Boskey 1995). To date, there is no consensus for a definitive function of any of them in the mineralized tissue (Marks and Hermey 2001). Most of these noncollagenous proteins are produced at different stages of the osteoblastic maturation, exhibiting a broad array of functions that include cell proliferation, cell-matrix interactions and mediation of the mineral deposition (serve as nucleator?). Small proteoglycans (i.e. decorin and biglycan) seem to regulate the collagen fibrillogenesis.

Type I collagen

Each molecule of Type I collagen is typically composed of two $\alpha 1$ chains and one $\alpha 2$ chain coiled

around each other in a characteristic triple helix. Both α1 and α2 chains consist of a long helical (coiled) domain preceded by a short N-terminal peptide and followed by a short C terminal peptide. The amino acids of the triple helix sequence consist of Gly-X-Y repeats. Due to this particular peptide sequence, each chain is coiled in a left handed helix, and the three chains are assembled in a right handed triple helix. The very small Gly residues are in the center of the triple helix while the lateral parts of the X and Y residues are on the surface of the helix. The molecule is secreted as a propeptide but N and C-terminal propeptides are rapidly cleaved by a specific protease on, or close to the cell membrane. After cleavage, the molecule still has short (15–20 AA) nonhelical domains at the C and N terminus of the three chains. These ends are called telopeptides and are very important for the fibrillogenesis. Each chain is ~1000 AA long and the molecule is composed of ~3000 AA; its length is 300 nm. In the extracellular space, the molecules assemble to form collagen fibrils (> 60µm long). In fibrils, molecules are parallel to each other, they overlap each other by multiples of 67 nm. There is a periodical gap of 40 nm between each molecule. This quarter staggered assembly explains the banded aspect displayed by the type I collagen on electron microscopy (Figure 17 B) (Von der Mark 1999; Rossert and de Crombrugghe 1996).

Post-translational modifications

The primary sequence of the molecule and the above mentioned steps of the collagen synthesis is identical in bones and elsewhere in the body. However, within rough endoplasmic reticulum of the matrix forming cells (osteoblasts, chondrocytes, fibroblasts…) and before formation of the triple helix, the α-chains undergo post-transcriptional modifications (glycosylation and hydroxylation) (Knott and Bailey 1998). About 100 proline residues and 10 lysine residues (in the Y position) are hydroxylated by specific enzymes (prolyl 3-hydroxylase and lysyl hydroxylases). The hydroxyproline and hydroxylysine are special amino acids which are virtually only found in the collagen molecules (Rossert and de Crombrugghe 1996).

Collagen cross-linking

In the extracellular space, during the fibrillogenesis, some specific lysine or hydroxylysine residue are deaminated by a lysyl oxidase. This enzyme deaminates the ε-NH_2 group, giving rise to an aldehyde derivative. The lysine oxidase is a copper dependent enzyme that acts on highly conserved amino acid sequences on the N and C terminal *telopeptides*. After this enzymatic step, subsequent reactions are spontaneous.

In bone the hydroxylysyl aldehyde spontaneously associates with ε-NH_2 groups from a lysine or hydroxylysine helical residues of neighboring collagen molecules, giving rise to the LKNL (lysino-5-ketonorleucine) and HLKNL (hydroxylysino-5-ketonorleucine). These cross-links (also called ketoimines, or reducible cross-links, or immature cross-links) are bivalent, linking the telopeptide from one molecule to the triple helix of another molecule (Figure 18). For biochemical dosage, they are stabilized by reduction with borohydride allowing hydrolysis and subsequent amino-acid analysis. After reduction, LKNL becomes **HLNL** (hydroxy-lysinonorleucine) and HLKNL becomes **DHLNL** (dihydroxy-lysinonorleucine).

The immature cross-links may further react with another telopeptide aldehyde and form mature trivalent cross-links. The hydroxylysyl pyridinoline (HP) is the most abundant of the mature cross-links found in a wide variety of tissues. It results from the reaction of the hydroxylysyl aldehyde of another collagen telopeptide with an immature HLKNL (Figure 19). The lysyl pyridinoline (LP) is less abundant, but found in significant amount in bone. It is thought to be formed by the reaction of a hydroxylysyl aldehyde with a LKNL cross-link. The ***HP*** and ***LP*** are the two forms of *pyridinoline* and just differ by the hydroxylation of the helical lysine residue included in the cross-link (Figure 19). In addition to the pyridinoline, ***pyrrole*** cross-links have been found in bone. These cross-links are thought to result from the reaction of a lysyl aldehyde with an immature cross-link. As for the pyridinolines, the pyrroles would form hydroxy-lysyl- and lysyl- variants depending on the type of immature cross-link reacting with the aldehyde (Kuypers et al. 1992). However, the current assays that use the Ehrlich's reagent cannot differentiate both forms of pyrrole.

The mature, trivalent cross-links (HP, LP and Pyrrole) are thought to have the capacity to form

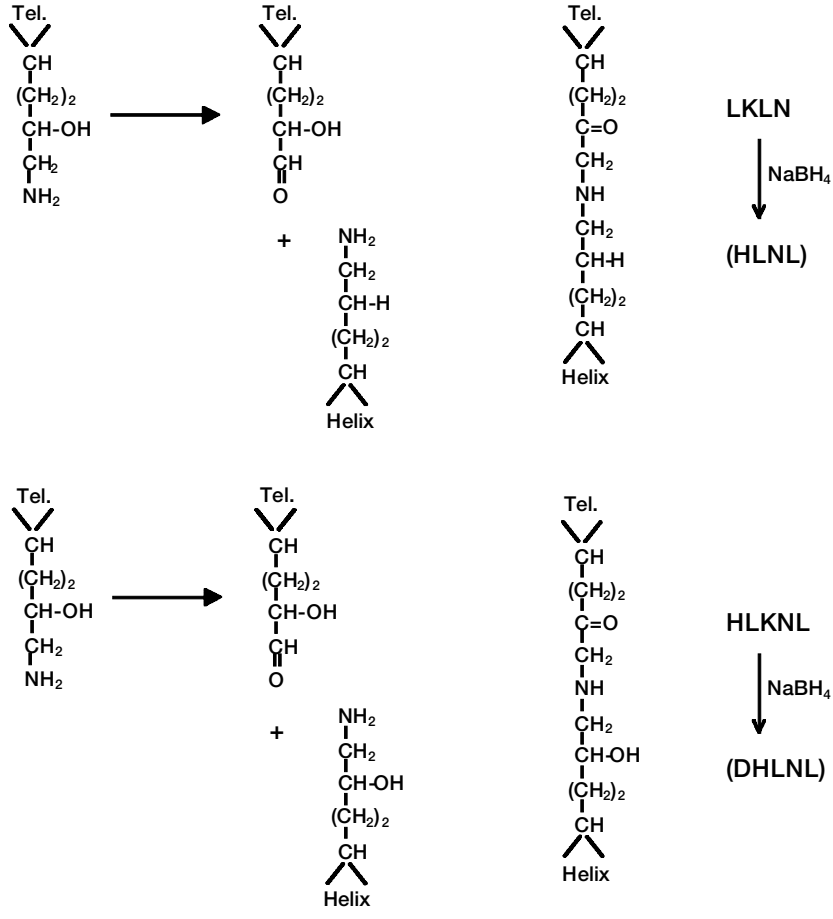

Figure 18. Formation of the immature cross-links. Telopeptide hydroxylysine residue is converted in an active aldehyde by the enzyme lysyl oxidase. This aldehyde then reacts with a helical lysyl residue to form a LKLN or with a helical hydroxylysyl residue to form a HLKNL cross-link. For the assay, these cross-links are reduced with borohydride (NaBH4) and form the HLNL and DHLNL.

intra- and inter-fibrillar cross-links (Figure 22).

Cross-link profile is tissue specific

When compared to other tissues (tendon, fascia, skin), bone collagen has a specific cross-link profile (Eyre 1996). In skin, for example, the telopeptide lysine residues are almost not hydroxylated. The divalent cross-links formed (called aldimine, not ketoimine) are much less stable than the ketoimines, and with collagen maturation, lead to the formation of histidine-containing cross-links (which are normally not found in bone). In contrast, in cartilage, the telopeptides and helical lysine residues involved in the cross-links are almost fully hydroxylated. As a consequence, the molar ratio of HP to LP is very high (HP/LP ratio ~50) and pyrrole is not found in cartilage.

Bone collagen stands in between those two extreme. Neither the telopeptide nor the helical lysine residues are fully hydroxylated. As a consequence, bone collagen a) can form pyrrole cross-links which are not found in skin or cartilage; and b) stands as having the lowest HP/LP ratio (~ 2 to 5). Additionally, bone contains relatively high amounts of immature cross-links (DHLNL and HLNL) contrary to soft tissues where they rapidly disappear as the tissue matures. The mineralization of the matrix has been invoked to account for that, by inhibiting the maturation of the cross-links. But this was has been disputed since in-vitro incubation of immature bone demonstrates the conversion of the ketoimines to pyridinolines and pyr-

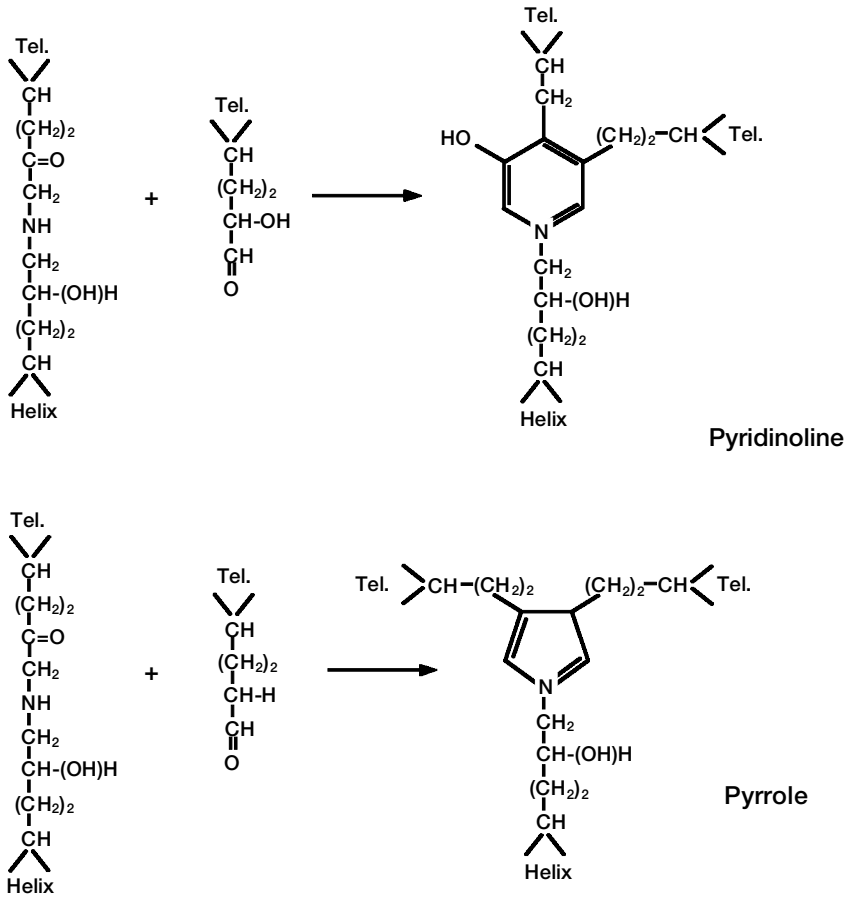

Figure 19. Formation of the mature trivalent cross-link. The pyridinoline result from the addition of a telopeptide hydroxylysine aldehyde to an existing LKNL or HLKN, the former resulting in the formation of LP and the latter in the formation of HP. The pyrrole cross-link results form the addition of a lysine aldehyde to these pre-existing bivalent crosslinks.

roles (Knott et al. 1995). These three features (Pyrrole, low HP/LP ratio and immature cross-links) are specific for bone collagen.

The pyrrole, HP and LP appear to be located at different ends of the molecule (Brady and Robins 2001; Hanson and Eyre 1996), supporting the concept of a direct influence of the type of cross-links on the fibrillar structure of the collagen.

Enzymatic control of the cross-link profile

As can be seen from the description of the cross-link pathway, the type of cross-link formed depends on the degree of hydroxylation of the lysine residues on both triple helix and telopeptides. In humans, at least three isoforms of the helical lysyl hydroxylase (HLH) have been identified (Passoja et al. 1998). Moreover, a telopeptide lysyl hydroxylase (TLH) has recently been identified, which is specific to bone tissue (Bank et al. 1999).

So, different types of fibrils can be formed based on exactly the same type I collagen molecule. Among other factors, the collagen properties depend on the amount and type of cross-links which are in turn controlled by specific enzymes. These enzymes yield specific cross-link profile in a given tissue, conferring specific function to this tissue.

General consideration

The heterogeneity of the collagen cross-linking in human tissues explain how an identical molecule can be the main structural protein of different tis-

sues. The bricks are the same but the construct is different. Although in extremely small quantity —10 µg/g of bone tissue—the cross-links may deeply influence the properties of the tissue.

The mineral matrix

Despite decades of research, the problems of the exact nature of the mineral phase and its deposition within collagenous matrix have never been satisfactorily solved (Grynpas 1993). As early as 1926, De Jong found that the X-ray diffraction patterns of bone mineral resemble that of poorly crystalline apatite. The mineral found in bone is an analog of the geologic mineral hydroxyapatite, $Ca_{10}(PO_4)_6(OH)_2$. Bone apatite is deficient in calcium and hydroxide, containing numerous impurities, the most abundant of which is carbonate. It forms relatively small crystals (20–40 nm in largest dimension).

As it is estimated that collagen fibrils occupy 85% of the volume of the matrix, the majority of the apatite crystals are probably located within the collagen fibers, while a minority are between the fibers. The long axis of the crystals lie parallel to the axis of the collagen fibers and earlier seeds of crystals have been found in the 'hole zone' of the fibers (Figure 17B), which have been considered as potential nucleation centers (Glimcher and Krane 1968). Actually, the main point is that both organic and mineral phases of bone are more or less *continuous*. A given type of cross-link profile may lead to a specific type of molecular and fibrillar packing that is necessary for mineralization of the matrix. In mineralizing turkey tendon, Knott et al. have shown that the removal of tendon-like type I collagen matrix and its replacement by a bone-like collagen matrix preceded the mineralization (Knott et al. 1997). Furthermore, there are indications that some glycoproteins—i.e. the bone sialoprotein (BSP-II), may initiate the mineralization acting as a nucleator (initiation of the mineral deposition).

Fatigue damage

The study of bone matrix has explored other aspects that need to be mentioned here. A lot of work has been done on the damage as a consequence of fatigue, although most studies have been performed on cortical bone. If a trabecula is loaded cyclically (with a slightly too high magnitude), the element may be damaged. Under the microscope damage may appear as 'diffuse alteration' or microcracks within the matrix and even complete fracture of the trabecula. Fractured trabeculae can heal through the formation of micro-calluses which are frequently seen in low density cancellous bone. The mechanical consequence of the damage is a reduction in stiffness. After microarchitecture, fatigue damage was considered as a hallmark of bone quality (Burr et al. 1997; Wenzel et al. 1996). We did not investigate this issue in our samples.

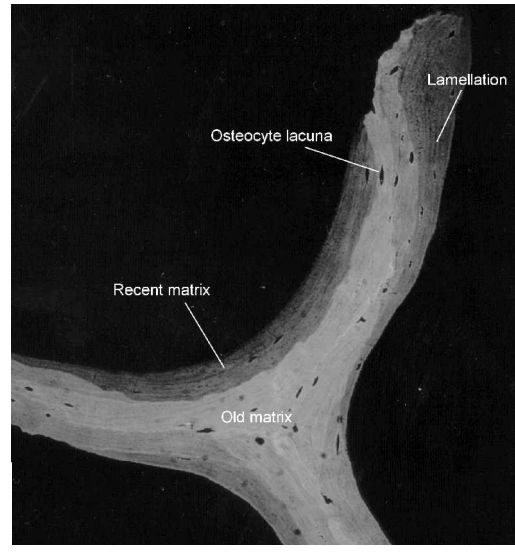

Figure 20. Backscattered electron image of vertebral trabeculae. One can see that the degree of mineralization varies within the trabeculae. Old matrix is more mineralized (whiter) than recently deposited matrix (darker).

Listing the parameters

Within a trabecula many parameters can change. These are listed in Table 5. Many factors in this list have been mentioned in our description of bone matrix. Note that some of them may interact with each other: The nature of the organic matrix is known to influence the type of mineral deposited; the osteocyte apoptosis probably results from fatigue damage and induces local remodeling…

Working hypotheses

In this section, we will investigate the cross-link profile of type I collagen in the vertebral cancellous bone. Consistently with Part I and II, we address the following hypotheses:

Table 5. List of the factors that may affect bone tissue

Structure of the tissue
Spatial orientation and thickness of the lamellae
Proper organization of the lamellae
Nature of the cement lines
Organic matrix
Biochemistry of the collagen fiber
Mutations in the amino acid sequence
Amount and nature of the cross-links
Quantity of collagen
Packing of the collagen molecules in the fibers
Spatial orientation of the collagen fibers
Content of non-collagenous proteins
Mineral matrix
Spatial repartition of the mineral
Mineralization profile
Size, shape and nature of the apatite crystal
Ca/P ratio
Extraneous ions like CO3, Mg, Na
Location of the crystals within and between the collagen fibers
Living material
Accumulation of fatigue damage
Microcracks
Diffuse damage
Microcallus
Amount of osteocytes
Osteocytes death
Functionality of the canaliculi

a) The cross-link profile of the vertebral cancellous bone is patient specific. In other words, different subjects have chemically different collagen, with differences in both the amount and the nature of the cross-links.
b) Quantitative parameters describing the collagen intermolecular cross-links can improve the prediction of bone mechanical properties (stiffness and strength).

Material and methods

We assessed the collagen biochemical properties of the 68 cylindrical samples that were not embedded in plastic and used for histology.

Biochemical analysis

The endplates of the 68 samples dedicated to the cross-link analysis were removed, leaving only pure cancellous bone for biochemistry. The samples were thoroughly washed under a jet of deionized water to remove bone marrow and blood cells, defatted in a 1 : 1 (v/v) chloroform-methanol solution, rinsed with methanol then with deionized water, and finally freeze dried.

Collagen determination

The amount of collagen was determined by hydroxyproline assay of an aliquot of the acid hydrolysate (6M HCL, 110 °C, 16 hr) using a continuous-flow Autoanalyzer (Burkard Scientific, Uxbridge, UK) based on the method of Grant (1965). The accuracy of the method was checked occasionally by the determination of hydroxyproline on the amino acid analyzer. The collagen content was calculated on the dry weight of the bone assuming 14% hydroxyproline in type I collagen. The resulting data were then used to calculate the cross-link values as mole per mole of collagen.

Immature cross-links and pyridinolines

The intermediate cross-links of the newly synthesized collagen were stabilized by borohydride reduction prior to acid hydrolysis, and both reduced and mature cross-links were determined after acid hydrolysis on a modified amino acid analyzer as previously described in detail (Sims et al. 2000; Sims and Bailey 1992).

Briefly, the bone samples were homogenized to avoid any possibility of differences due to thickness of the bone, suspended in phosphate buffered saline, and reduced with potassium borohydride. The samples were washed, freeze-dried, reweighed, and hydrolyzed in 6 M HCl for 24 hours at 110°C in screw topped glass hydrolysis tubes (Medline Scientific, Oxon, UK). The excess acid was removed by freeze-drying, and the residue was dissolved in 0.5 ml of distilled water.

The hydrolysates were initially separated on a CF1 (Whatman, Kent, UK) cellulose column to remove the non-cross-linking amino acids. The samples were assayed for the borohydride reduced form of immature cross-links, i.e., hydroxylysinonorleucine (HLNL) and dihydroxylysinornorleucine (DHLNL) together with the stable mature hydroxylysyl-pyridinoline (HP) and lysyl-pyridinoline (LP) cross-links, using a modified gradient on an amino acid analyzer (Alpha Plus, Pharmacia, Loughborough, UK). The location of the cross-links on the analyzer had previously been confirmed with samples of authentic cross-links pre-

pared in the laboratory. Quantification of the cross-links was achieved using ninhydrin color reaction and their known leucine equivalents. The ratio between both types of pyridinoline (HP / LP ratio) was computed.

Pyrrolic cross-link

Bone matrix (100 mg) was dispensed into polypropylene tubes (Sarstedt, Leicester, UK) and initially decalcified by suspension (20mg/ml) in 0.5 M tetra-sodium EDTA, pH 7.5 for 3 days at 4 °C. The EDTA was decanted after centrifugation (10.000 rpm) and the decalcified matrix was resuspended in distilled water, shaken, and subsequently centrifuged (10.000 rpm). After repeating this wash step, 1200 µl of 0.1 M TAPSO, pH 8.2, was dispensed into each tube and the sample heat denatured at 100 °C for 30 minutes and then allowed to cool to 37 °C. Samples were then treated with 1000 units of trypsin (TPCK-treated) dispensed from a trypsin stock (5000 units/ml TAPSO buffer) and left to digest by shaking gently for 18hr at 37 °C. The pyrrole content of the digest was assayed by reaction with p-dimethylamino-benzaldehyde (DAB) using a micro-titer plate format (Bailey et al. 1999) (Micro test III flexible plate, Becton Dickinson, California, USA). Quantification was facilitated by the inclusion of a 1-methyl pyrrole (Aldrich, Dorset, UK) standard (range 1–10 mmol/L) prepared from a stock solution (50 mM in ethanol). A 50 µl aliquot was removed for total collagen content by hydroxyproline assay described above. A further 250 µl of each sample was combined with 50 µl of DAB (11.4% w/v in 60% perchloric acid). Within 15 minutes of adding the DAB, all samples were filtered employing a 0.2 µm syringe filter (13 mm, HPLC technology) and 180 µl of the sample was dispensed into a 96-well microtiter plate and read at 570 nm using a microtiter plate reader (Labsystems Multiskan MCC 340).

The pyrrole content of the bone digests was calculated based on the Extinction Coefficient of 25,000 for 1-methyl pyrrole (Scott et al. 1981) and expressed as moles of pyrrole per mole of collagen based on the hydroxyproline assay. The ratio between immature and mature cross-links (immature / mature ratio) was calculated as [DHLNL + HLNL] / [Pyrrole + HP + LP].

Table 6. Biochemical parameters

Parameter	n	Mean	SD
Collagen (%)	63	26.3	1.6
HP (mol/mol)	63	0.13	0.04
LP (mol/mol)	63	0.07	0.03
HP / LP ratio	63	1.99	0.68
Pyrrole (mol/mol)	63	0.09	0.02
DHLNL (mol/mol)	62	0.12	0.05
HLNL (mol/mol)	62	0.08	0.02
DHLNL / HLNL ratio	62	1.65	0.74
Inter / Mature (–)	62	0.69	0.22

Density and mechanical properties

In addition to the collagen properties we used the strength, stiffness and density measurements which were obtained as described in part I.

Statistical analysis

Hypothesis 1: We used the same statistical approach as in part II. Briefly, we checked if the biochemical parameters were compared to the density using simple correlation analysis. Then, the biochemical parameters were computed in the mixed model to enhance those that varied significantly between subjects and between locations. η^2 values and estimated marginal means are reported. Note that no covariates were used since the correlation with density was very low.

Hypothesis 2: The relationship between mechanical properties (stiffness and strength) and biochemical parameters was explored using a stepwise multiple regression model. The density was always introduced as first predictor.

Results

Intermolecular cross-links

Both reduced intermediate cross-links, HLNL and DHLNL were identified, the latter being approximately double the concentration of the former. The major cross-link in these adult bone samples was the mature HP, the LP being about half that of the HP value. The total pyridinolines amounted to about 0.2 to 0.3 moles cross-link per mole of collagen, whilst the pyrrole accounted for about 0.1 mole per mole collagen (Table 6). None of the biochemical parameters correlated with density.

Table 7. Correlation between the collagen parameters and the mechanical parameters

	Stiffness (MPa)	Strength (MPa)	Ultimate strain (%)
Collagen (%)	0.25	0.26 [a]	–0.07
HP (mol/mol)	0.09	0.25	0.37 [b]
LP (mol/mol)	-0.20	-0.06	0.39 [b]
HP / LP ratio	0.47 [c]	0.40 [b]	–0.16
Pyrrole (mol/mol)	0.04	0.09	0.03
DHLNL (mol/mol)	–0.09	0.01	0.14
HLNL (mol/mol)	–0.11	–0.09	–0.09
DHLNL / HLNL ratio	–0.12	0.00	0.19

Results of the multiple regression. After controlling the (major) effect of the density, the biochemical data of each sample is introduced in the model. Correlation coefficients represent the part of variability explained by these biochemical data (partial correlation, r values). The improvement of the prediction due to the introduction of the biochemical parameter is tested.
Key: [a] $p < 0.05$, [b] $p < 0.01$, [c] $p < 0.001$

All biochemical parameters were subject specific (Figure 21). About 70% of the variance of the collagen content depended on the individual subject (η^2 value). The most subject specific aspect of the collagen cross-link profile was the HP / LP ratio as well as the concentration of LP in the bone (with 82 and 81% of the variance associated with the subject). The sample site within the vertebral body (anterior, posterior or external) had no systematic influence on the biochemical parameters. Only a small part of the variance of the HP and LP concentrations (10%) was dependent on the level the samples were taken from, thoracic, thoraco-lumbar or lumbar.

Biochemical parameters and mechanics

The regression analysis indicated that, after controlling the major effect of density, a substantial part of the 'unaccounted variance' was explained by the biochemical properties of the collagen (Table 7). The HP / LP ratio was found to be a significant predictor of the stiffness ($r = 0.47$, $p < 0.001$) and strength ($r = 0.40$, $p = 0.001$). The concentration of pyridinoline cross-links (HP and LP) in the collagen were also correlated with the ultimate strain ($r = 0.39$ and $r = 0.40$ respectively, $p < 0.01$) . Neither the intermediate cross-links determined by borohydride reduction (DHLNL or HLNL), nor the pyrrole cross-links correlated with any of the three mechanical parameters.

As the cross-link profile was a subject specific data, we applied the regression procedure to the mean values of each subject (n = 9). The HP / LP ratio was still significantly predictive of the stiffness ($r = 0.73$, $p < 0.05$) and the strength ($r = 0.65$, $p < 0.05$). For the prediction of the ultimate strain the concentration of LP remained a valuable predictor ($r = 0.66$, $p < 0.05$).

Discussion

The data presented here suggest that the type of collagen cross-linking contributes significantly to the prediction of the biomechanical properties of cancellous bone from the vertebral bodies.

Subject to subject variations of the cross-link profile

Previously published data

Some studies have reported changes in the nature of the collagenous matrix in the context of specific disease—i.e., osteoarthritis (Mansell and Bailey 1998; Li and Aspden 1997), osteoporosis (Oxlund et al. 1996; Bailey et al. 1992). As far as we know, there has been no demonstration of substantial differences between 'normal' patients, as shown in this section (Figure 21). This is mainly due to the fact that, usually, only one or two samples were harvested per patient. However, the range of variation that we observed is compatible with the data reported on the iliac crest (Bailey et al. 1999) or on the femoral epiphysis or cortex (Eyre et al. 1988). Both studies observed some variability in the cross-link content of the samples. But they could not demonstrate whether these differences were due to random errors—i.e. during the assay, or really to differences between the patients. Our experimental design (with measurement repeated up to 8 times in the same subject) allowed us to conclude that the vertebral bone of different patients had different cross-link profiles. Note that the above mentioned studies showed that there was no change in the bone collagen properties with age, in adults. In the younger (from 0 to 20 years), Eyre et al. (Eyre et al. 1988) showed that there was a progressive decrease of the immature cross-links

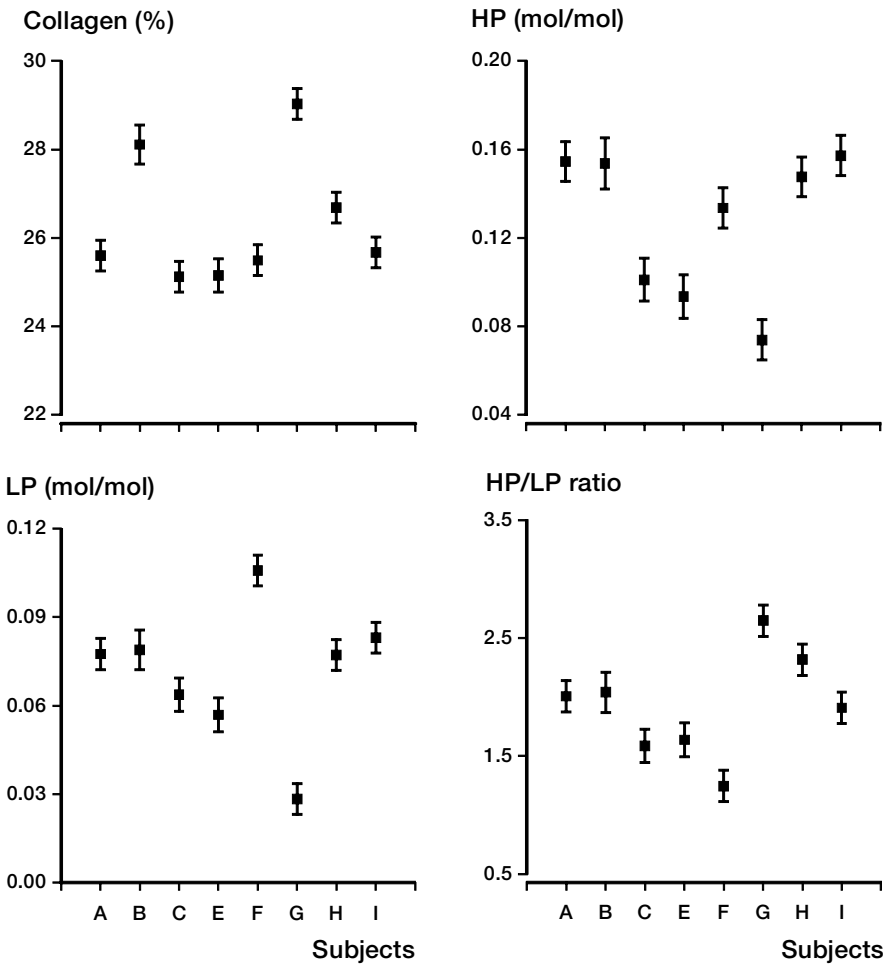

Figure 21. Variation of collagen properties among subjects. Most of the aspects of the collagen cross-link profile were patient specific.

(DHLNL and HLNL) associated with a progressive increase of the mature cross-link (for instance HP and LP).

The nature of bone tissue

So, the biochemical nature of the collagenous matrix varies significantly from patient to patient. When considering the quest for new predictors of bone strength, we can conclude that the collagen properties fulfill the first requirement as stated in part I.

It is somewhat puzzling to observe that the concentration of cross-links, that are considered as important characteristics of bony tissue, can vary in a significant proportion. The amount of LP, HP or pyrrole and the immature / mature or HP/LP ratios were found two times higher in some patients compared to others (Figure 21). As all these patients actually had correctly mineralized cancellous bone, one could conclude that the mineralization does not require a really precise profile to occur. Different matrices in terms of collagen cross-links do mineralize.

Urinary pyridinolines

The practical consequences of such observations should not be underestimated. Urinary pyridinolines have become the most commonly used marker of bone resorption for clinical research (Eyre 1996). Urinary LP values are generally considered to be more specific than HP for bone collagen, because of its higher abundance in bone than

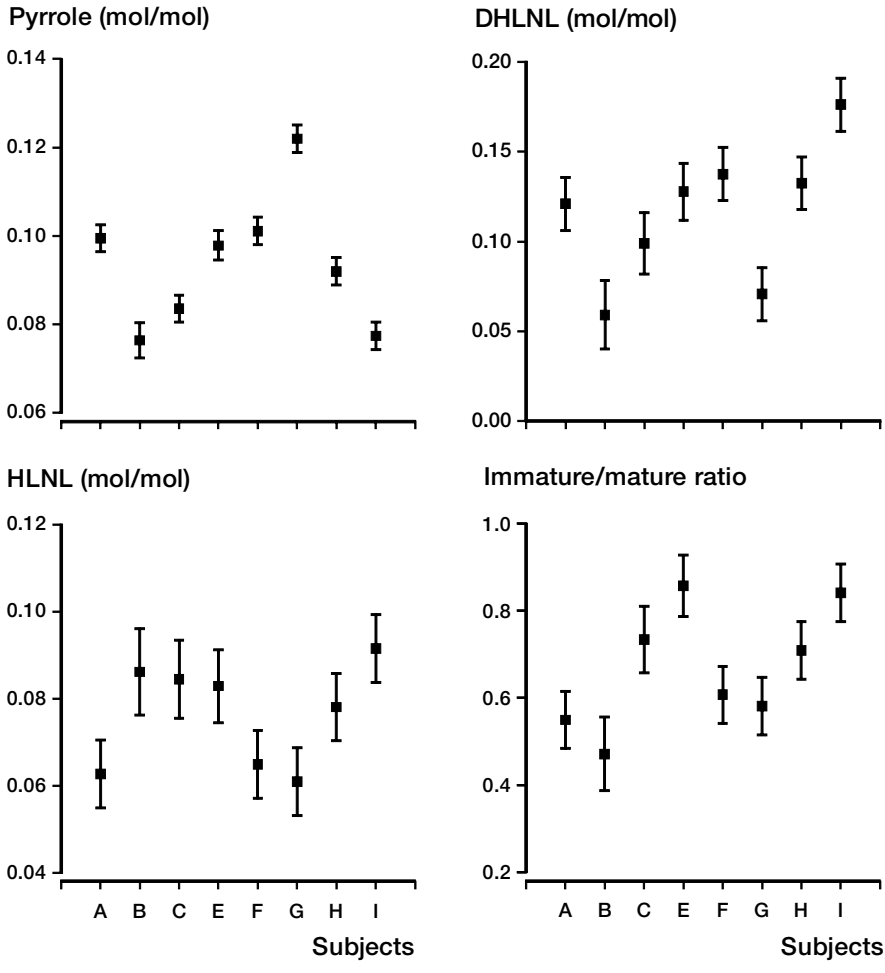

Figure 21. Continued.

in other collagenous tissues. Both free or peptide bound LP can be quantified in urine, the amount released daily from bone depending on the amount of bone collagen degraded by the osteoclasts.

On direct analysis of the vertebral bone collagen, the concentration of LP varied considerably among subjects (Figure 21). For example, subject G had 0.03 ± 0.005 (mean ± SD) moles of LP per mole of collagen while subject F had 0.11 ± 0.020. If both of them degrade the same quantity of vertebral bone (in grams), the first will release much less LP than the second. Consequently, the urine cross-links are certainly sufficiently sensitive to follow the evolution of a given patient, but possibly not to compare the metabolic activities of different patients.

The variability of the HP/LP ratio between subjects is due to the different degree of hydroxylation of the specific lysines residues involved in cross-linking (Figure 18 and 19). The present observation that different subjects had different HP/LP ratios indicates that the activity of the triple helix hydroxylase(s) vary from patient to patient. Similarly, the variations in pyrrole content indicates that the activity of the telopeptide hydroxylase that acts on the lysine residues included as second aldehyde in the pyrrole varies. Whether this is genetically controlled or depends on external conditions is currently unknown. Genetic control is more probable than environmental control. Puustjarvi et al. (1992) have shown, on a dog model, that intensive exercise (40 km/day) did not have any influ-

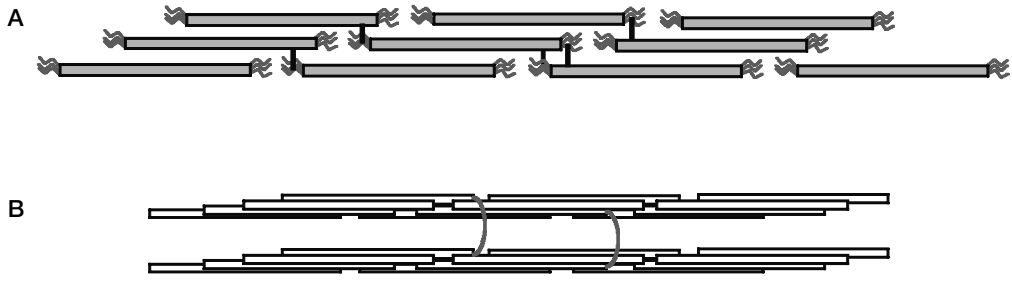

Figure 22. A schematic representation of a proposed location of the enzymatic cross-links. (A) Immature, bivalent cross-links as well as pyridinoline are found within the microfibrils, forming an intrafibrillar cross-links. (B) The pyrrole cross-link may form a linkage between two parallel microfibrils, forming interfibrillar cross-link (10). Even a small amount of crosslinks can modify the structure of the collagen and hence its function. (Modified from Knott et al. 1998, with permission from Elsevier Science).

ence on the pyridinoline content of vertebral cancellous bone.

Cross-links and mechanics

Our results indicate that a significant part of this 'unaccounted' variance was related to differences in matrix composition of the trabeculae. The HP / LP ratio was a good predictor of stiffness and strength of the bone cylinders. Samples with a high HP / LP ratio possessed a better *bone tissue quality* than samples with a low ratio. As this biochemical parameter varied significantly across subjects (Figure 21), subjects with a higher HP/LP ratio had a relatively stiffer and stronger bone.

The strength of the HP or LP covalent bond is considered to be the same as the only difference between these two cross-linking amino acids is only the presence or absence of an hydoxyl group. We do not believe that the HP/LP ratio can account by itself for the difference in mechanical properties. Its effect on the strength must be mediated by some of the parameters listed in table 5. For example, difference in the extent of hydroxylation of the triple helix could lead to different packing of the fibrils.

The non-collagenous proteins are known to contribute significantly to the mineralization process (Robey and Boskey 1995). Knott et al. have previously shown that the lysyl hydroxylation in type I collagen of tendon was reduced on mineralization of the tendon, suggesting that the change might be associated with the mineralization process (Knott et al. 1997). To speculate further, one could consider the hypothesis that the type of cross-link present in the collagenous matrix may also influence the quality and extent of mineralization (i.e. the size and shape of the crystals), which in turn could affect the mechanical elastic properties of the bone. It is generally considered that the mineral accounts for bone stiffness. Thus, the key point in understanding our results may rely in the quality of the mineral present in our samples. Further inquiries in that field are certainly needed.

The absence of any correlation of the modulus or compressive strength with cross-links in human iliac crest bone (Bailey et al. 1999) is unclear and may be due to the absence of specific loading direction of the fibers, which has recently been shown to be important (Puustjarvi et al. 1999) or to the use of different protocols for mechanical testing. Knott et al. (1995) previously reported a relationship of strength with the pyrrole cross-link in avian bone, but this may be related to the fact that the concentration of the pyrrole was double that of the pyridinoline in these animals, while in human vertebral cancellous bone, pyrrole was less abundant than pyridinoline. Additionally, the avian cortical bone was tested in three point bending which leads to a tensile mode of failure.

Biochemical properties versus microarchitecture

The design of the study allows us to compare the relative capacity of histological and biochemical analyses to improve the prediction of bone strength. On one side of the vertebral body, density and microarchitecture were histologically deter-

mined. On the other side of the vertebral body, the pQCT was used to measure the density and the cross-links were assayed. BV/TV and pQCT density had the same correlation coefficient with stiffness and strength ($r \sim 0.90$). We had better capacity to predict the stiffness using density and HP/LP ratio ($r^2 = 0.87$) than using i.e. BV/TV and Star ($r^2 = 0.81$). The prediction of strength using density and HP/LP ratio ($r^2 = 0.84$) was apparently better than using i.e. BV/TV and Star ($r^2 = 0.80$). However, we must stress that our sampling and statistical methods are not adequate to *demonstrate* that fact.

Limitations and strengths of the study

Our study was strong in that we directly realized all measurements on human vertebral cancellous bone. The use of human material from an anatomical site that has the highest risk of fracture with aging is certainly important if we intend to draw clinically relevant conclusions. This is much more difficult with animal models. The biochemical and mechanical analysis were performed on the same samples. Our sampling strategy was rigorous and proved its sensitivity to the within-subject variations in the structure or density.

Conclusion

In this study, we improved the prediction of the biomechanical properties of vertebral cancellous bone by combining pQCT (density) data and direct collagen cross-link assessment. As both density measurements and pyridinoline levels (HP / LP in urine) are accessible in clinical practice, our observations open an interesting way of progress in the prediction of fracture risk.

Part IV: Unexpected finding on cross-links and morphometry

Introduction

A common point

In part II and III we explored the nature and the 3D structure of the vertebral cancellous bone as potential predictors of the biomechanical behavior. There is a common point between the biochemical parameters listed in part III and the architectural parameters listed in part II. They both result from bone remodeling. As described in the introduction of part III, bone is a living tissue. Continuously small volumes of bone are removed and subsequently replaced by new matrix. It is estimated that as much as 8–25% of the bone tissue is renewed every year (Parfitt 1988). Such a turn-over rate is fairly high, much higher than in other connective tissue (tendon, skin dermis…).

The complex microarchitecture of the trabeculae, or at least its persistence, ultimately depends on the location and shape of the resorption lacunae and on the ability of the osteoblasts to refill these cavities. For example, deleterious plate perforations or bar disconnections may occur during the resorption phase of the remodeling cycle resulting in a definitive change in the structure (Parfitt et al. 1983). There is also a clear link between the nature of the bone matrix and bone remodeling. Changes in the quality of the bone formation may alter the bone matrix (e.g., osteomalacia) and changes in the nature of the matrix may, in turn, influence bone resorption (e.g., therapy with bisphosphonates).

Bone remodeling, the osteoid bone

A layer of osteoid bone is a hallmark of local remodeling activity. Little or no osteoid bone means low or no remodeling while a lot of osteoid generally reflects a high remodeling activity. The amount of osteoid bone can be assessed by morphometry on adequately stained thin sections. The bone surface covered by osteoid can be measured, as well as the mean thickness of those osteoid layers. The volume of osteoid, compared to the volume of bone can also be measured. Authors have shown that the osteoid indices reflected other apposition data as obtained with tetracycline labeling: The osteoid thickness reflects the adjusted apposition rate; the osteoid surface, the activation frequency; and osteoid volume, the bone formation rate (Parfitt et al. 1997). Only one study reports the quantification of osteoid on human vertebral cancellous bone (Alexiades et al. 1990).

To date there has been no study comparing the collagen cross-link profile of cancellous bone with microarchitectural data and new bone formation indices. Correlating the nature of the bone material deposited with the final structure obtained may help in understanding the biology of bone remodeling. In this study, we had the opportunity to combine both types of investigation and to address the following questions:

a) Is there a specific cross-link profile associated with low bone density?
b) Is there a relationship between the 'maturity' of the cross-links and the new bone formation indices (that measure the amount of bone tissue that is not yet mineralized)?
c) Is there a correlation between the structural organization of the trabeculae (estimated by the morphometrical parameters) and the chemical nature of its organic matrix (estimated by its cross-link content)?

Materials and methods

Data collection

68 cylinders on one side were used for microarchitecture (see part II) and osteoid indices, and 68 paired cylinders from the other side were used for biochemical analysis (see part III). As mentioned part II, in addition to the Von Kossa stained thin section, another thin section was stained with Goldner Trichrome which shows the mineralized tissue in green and the osteoid non-mineralized tissue in red.

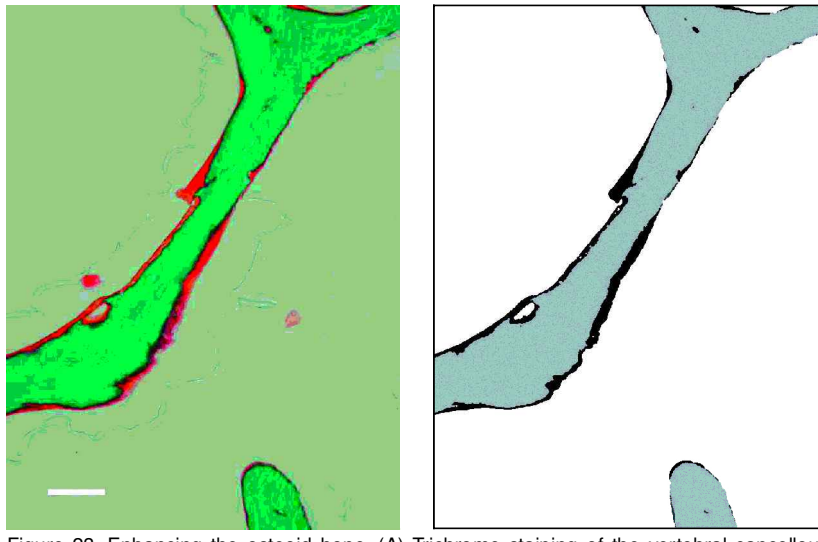

Figure 23. Enhancing the osteoid bone. (A) Trichrome staining of the vertebral cancellous bone from a patient with a relatively high amount of osteoid bone (seen in red). Scale bar (in white) is 100 µm. About 10,880 of such digitized pictures were used to determine the new bone formation indices. The computer automatically identified osteoid layer. (B) To control the result of this selection, a gray image was saved and compared with the original image. When an artifact or default of staining compromised the selection, the corresponding surface and perimeter data were not used to calculate the osteoid surface (OS/BS), osteoid thickness (O.Th) or osteoid volume (OV/BV) of that sample.

Goldner trichrome: new bone formation indices

For the detection of the osteoid layers a higher magnification is required. We used an optical microscope (Axioplan Zeiss, Germany) with a motorized stage controlled by a digital pad. Each slice was scanned to obtain 40 contiguous pictures (covering 60% of the section). The size of each picture was 1 mm × 0.75 mm. Pixel size was 1µm, image size was 1024 pixels × 768 pixels (Figure 23A). The same settings of the digital camera were used for all the 10,880 images. A home-made macro was built using Qwin to process color images. A constant color threshold (on the RGB components of the color signal) was used to differentiate the tissues. When combined to a sequence of logical algorithms (i.e., a red osteoid surface has to be close to a mineralized green surface) the macro correctly segmented the image. The 10,880 images were processed over a single computing session (lasting 60 hours). The output data (the surfaces and perimeters) and a gray level image representing the selection (Figure 23B) were saved 'on line'. The operator reviewed all trichrome images and the gray selection to validate the results and the output data. When the slice was locally damaged, cracked or incorrectly stained, the image was not included. For 9,420 images the operator considered that the selection was useful and valid. When less than half of the images (<20/40) were valid, the value for that slice was not considered, leading to the loss of 15 slices / 272. For a given cylinder, there were always at least 3 slices to estimate the osteoid. The total, bone and osteoid surfaces and perimeters were summed for a given slice to compute the following new bone formation parameters: the osteoid volume (OV/BV, %), the osteoid thickness (O.Th, µm) and the osteoid surface (OS/BS, %). O.Th was derived from the surface / perimeter data. A cylinder was characterized using the mean of the values coming from 4 (or 3) valid slices.

Data processing and statistical analysis

SPSS 10.0 (SPSS Inc., Chicago, IL) was used for data processing and statistical analysis.

First, the osteoid parameters were introduced in the mixed model to determine the effect of the location variables and the between subject differences.

A total of 12 histological parameters (9 structural and 3 osteoid) describing 68 cylinders were

Table 8. Correlation between histomorphometry and biochemistry (r values)

	Collagen biochemical parameter							
Histomorphometry	Collagen (%)	HP (mol/mol)	LP (mol/mol)	HP / LP ratio (–)	Pyrrole (mol/mol)	DHLNL (mol/mol)	HLNL (mol/mol)	Immature / Mature (–)
Amount of bone								
BVTV (%)	–0.23	–0.11	–0.2	0.15	–0.02	0.18	0.20	–0.39 [b]
Structural parameter								
Tb.Th (µm) [d]	0.33 [b]	-0.55 [c]	–0.32 [a]	0.04	0.65 [c]	–0.19	–0.29 [a]	–0.08
Tb.N (–/mm^2) [d]	–0.24	0.51 [c]	0.22	0.07	–0.57 [c]	0.17	0.27 [a]	0.08
Tb.Sp (µm) [d]	0.22	–0.51 [c]	–0.24	–0.05	0.57 [c]	–0.19	–0.21	–0.06
TSL (mm/mm^2) [d]	–0.18	0.54 [c]	0.23	0.12	–0.54 [c]	0.26 [a]	0.26 [a]	0.12
Nd (–/mm^2) [d]	–0.11	0.23	0.05	0.02	–0.49 [c]	0.00	0.27	0.07
Fe (–/mm^2)	–0.26 [a]	0.30 [a]	0.17	–0.14	–0.54 [c]	–0.14	0.21	–0.10
Nd/Fe (–) [d]	0.26 [a]	–0.11	–0.20	0.26 [a]	0.11	0.18	0.10	0.24
Star (mm^2) [d]	0.19	–0.48 [C]	–0.24	–0.02	0.46 [c]	–0.15	–0.23	–0.01
New bone formation indices								
OV/BV (%)	0.07	0.31	0.14	0.00	–0.36 [b]	0.15	0.20	0.03
O.Th (µm) [d]	–0.03	–0.01	0.08	–0.11	-0.13	0.12	0.14	0.17
OS/BS (%)	0.12	–0.28 [a]	0.12	0.00	–0.29 [a]	0.16	0.17	0.03

The r value is an estimate of the part of the total variability (in the morphometrical parameter) explained by the biochemical parameter. Significant correlations are found between the amount of pyrrole or HP crosslinks and multiple structural parameters.
Key: [a] $p < 0.05$, [b] $p < 0.01$, [c] $p < 0,001$, + means that the correlation is positive, – that it is negative,
[d] Indicates that the BV/TV was first introduced in the model, meaning the the r is rather a partial correlation coefficient.

compared to 8 biochemical parameters describing the 68 corresponding cylinders.

The relationship between the variables was investigated using a stepwise regression model. The morphometrical parameter was the independent variable. When a morphometrical parameter was strongly linked to the BV/TV (as was the case for most of them, see Table 2), two covariables were used in the model: BV/TV was introduced first, followed by the biochemical parameter. Using this procedure, the model explored the relationship between the biochemical parameter and the variance of the morphometrical parameter that was not explained by the BV/TV and partial correlation coefficient (r) are reported. Due to the large number of correlations tested only those with $p < 0.01$ were considered.

To illustrate the 'purely morphometrical information', (see part II) we used the residues of the regression between the parameter (i.e. Tb.Th, TSL…) and the BV/TV as raw data (indicated with an asterisk: Tb.Th* or TSL* in Figures 21 and 24A). For example, a value of 15 µm of Tb.Th* means that the trabeculae of that given sample were 15 µm thicker than expected knowing the BV/TV.

Results

Density and cross-links

Although the sampling covered a wide range of density (BV/TV range: 4.6% to 15.6%), none of the collagen properties correlated with BV/TV except a mild correlation (r = 0.39) between the immature / mature ratio and the BV/TV (Table 8).

Osteoid and cross-links

We found osteoid bone in all samples. The new bone formation indices were not correlated to the BV/TV except the O.Th ($r = 0.44$, $p < 0.05$). Regarding the osteoid parameters, two subjects had 6% of OV/BV while the others had 2.7 to 0.8 %. These parameters did not vary significantly within a subject and no anatomical pattern was enhanced by the mixed model. None of the biochemical parameters correlated with either the O.Th or OS/BS. There seemed to be less OV/BV when high pyrrole concentration were noticed (r = –0.36). More specifically, there were no more immature cross-links (DHLNL or HLNL, immature /mature ratio) when the new bone formation rate was important.

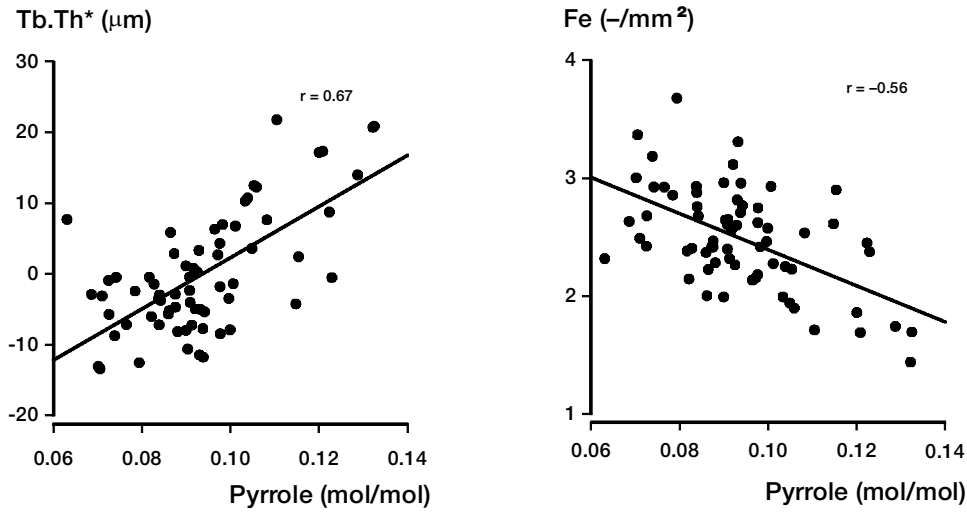

Figure 24. Correlation between the concentration of pyrrole cross-link and the structure (n = 68). After correction for the (dominant) BV/TV influence, the trabecular thickness (Tb.Th*, μm) of a given cylinder correlated positively with the concentration of pyrrole (A). The number of free-ends (Fe, –/mm²) was negatively correlated to the concentration of pyrrole (B).

Structure and cross-links

Samples with a high pyrrole concentration had relatively thick trabeculae (Tb.Th*: $r = 0.65$ $p < 0.001$, see Figure 24A), that were less numerous (Tb.N: $r = -0.57$ $p < 0.001$) and more widely spaced (Tb.Sp: $r = 0.57$ $p < 0.001$). Furthermore, the trabecular network was significantly less complex, spreading over a smaller length (TSL: $r = -0.54$ $p < 0.001$) with less nodes (Nd: $r = –0.49$ $p < 0.001$) and less dis-connections (Fe: $r = –0.56$ $p < 0.001$, see figure 24B). Finally, the star surface was smaller when the pyrrole values were high (Star: $r = 0.46$ $p < 0.001$). All these correlations are consistent with the concept that high pyrrole means thick, simple and disconnected structure while low pyrrole means thin, complex and more connected structure.

The opposite relationships were noted for the HP concentration, but, overall they were less significant and not significant for the Nd and Fe (Table 8). It should be noted that the concentration of pyrrole was negatively correlated to the concentration of HP ($r = –0.33$).

Subject specific data

All the investigated parameters were strongly subject-specific as a significant between-subject variance ($p < 0.001$) was detected in the mixed model (see part II). When the Von Kossa-stained thin sections of two subjects with the same BV/TV were compared, differences in the structural organization of the trabeculae were obvious. Considering Figure 13 in part II the subject H with a thin structure had low pyrrole concentration and relatively high HP while subject G with a thick structure had relatively high pyrrole and low HP.

Discussion

Our present observations indicate a relationship between the nature of the bone collagenous matrix, in particular, the concentration of the pyrrole cross-link, and the structural organization of the trabeculae. A high pyrrole content was found to be correlated with a thick, simple, disconnected structure, whilst low pyrrole reflected thin, complex and a more connected structure. In contrast, the properties of the collagenous matrix did not correlate with the density (BV/TV) nor with the new bone formation indices.

Three hypotheses

The basis of the correlation of bone microarchitecture and pyrrole cross-link presents us with a challenging question. The observations reported here

were strictly unexpected. Indeed, we are unable to explain why both set of variables were correlated. Consequently, most of the following comments are speculative and should be considered cautiously.

First, we observed that the structural organization of the vertebral cancellous bone and most of the collagen properties were subject dependent. Knowing that the cancellous bone is continuously resorbed and rebuilt (25% of the vertebral bone mass / year) one can guess that both are under the influence of a control mechanism. The **controlling factor** may be genetic (different structures or chemical composition being the expression of different phenotypes) or a strong environmental stimulus (see dicussion in part III).

The formation of the pyrrole depends on reduced telopeptide lysine hydroxylation, both on specific triple helical lysine and the telopeptide lysine. Pyrrole cross-links predominate at the amino terminus of the molecule whilst pyridinoline predominate at the carboxy terminus, indicating a further specificity of the lysine hydroxylase (Brady and Robins 2001; Knott and Bailey 1998; Hanson and Eyre 1996).

To explain a correlation between the cross-link profile and the morphometry, three hypotheses are presented in Figure 25:

i) In the first hypothesis, both structure and cross-links are under the same control. This would be the case if haphazardly, both controlling genes were very close to each other with a combined high or low expression. In such a case, the biological meaning of our observations is weak.

ii) In the second hypothesis, the control acts on the structural organization of the trabeculae and, if the biological system builds a given structure, then, de-facto, the pyrrole is high or low. For example, one may think that you have a given structure *because* turn over is very high or low, and that a given amount of osteoid yields a given amount of pyrrole. Note that we measured the osteoid / new bone formation indices only to check whether the amount of osteoid was the key between cross-links and morphometry. Our data do not support this precise idea.

iii) Finally, the cross-link content of the bone matrix may be responsible for the structural organization. It is possible that an individual subject has a given cross-link profile because of a given expression of the genes coding these enzymes. Now, why would a given organic matrix induce a given structure?

a) Because of the osteoclasts: Certainly the cross-linking of collagen affects the susceptibility of the fibers to proteolysis (Vater et al. 1979). However, whether the different mature cross-links influence the ability of the degradative enzymes from the osteoclast to degrade the fiber is debatable. It is therefore conceivable that the presence of the pyrrole cross-link may affect the rate of catabolism of bone collagen by MMP's and cathep-

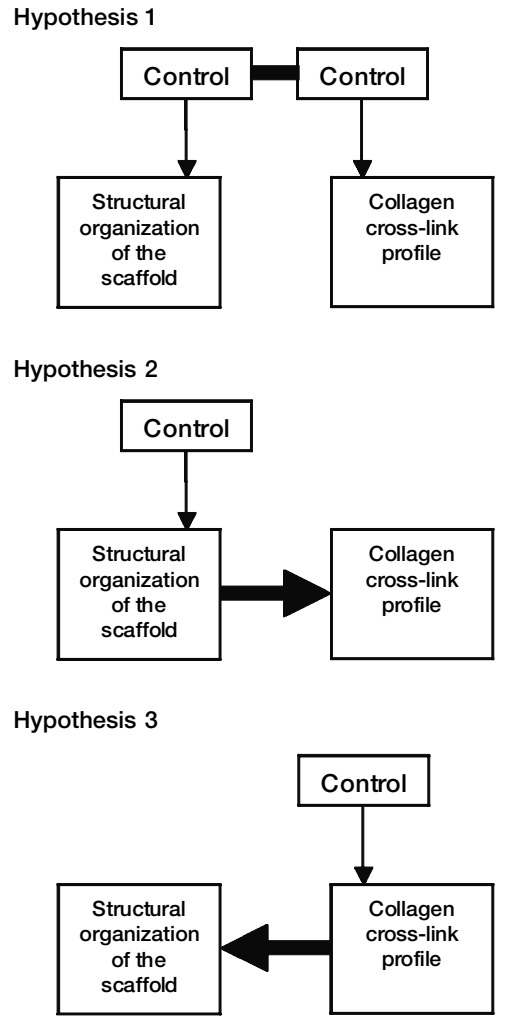

Figure 25. Three possible hypotheses that would explain the observed relationship between the morphometry and the collagen cross-links (for detail see text).

sin K. Deeper resorption cavities could progressively (over decades) modify the architecture.

b) Because of the osteoblasts: The activity of the lysyl hydroxylase appears to be related to the metabolism of the collagenous structural matrix, being high in rapidly growing bone, healing fractures or disease (Mansell and Bailey 1998), hence the presence of the pyrrole cross-links in the thick structures could indicate a low turnover of the collagenous matrix in these situations. It has been previously proposed (Knott and Bailey 1998) that pyrrole may be an interfibrillar cross-link whilst pyridinoline is intrafibrillar (Figure 22). It is possible, therefore, that pyrrole is capable of building up and stabilizing thick trabeculae compared to higher turnover, thinner, pyridinoline cross-linked trabeculae. Indeed, very high lysyl hydroxylase levels in highly metabolizing collagen have been shown to lead to thin fibers (Batge et al. 1992) and they possess pyridinoline as the predominant cross-link.

A biological marker

The practical consequences of the observed direct correlation between the pyrrole cross-link and the structural parameters could prove important. For example, studies have reported that the addition of the structural parameters to bone density measurement improved the ability to differentiate between patients with and without vertebral fractures (Dempster 2000; Legrand et al. 2000; Gordon et al. 1998). Nowadays, most clinical investigators concerned with bone quality have access to densitometry (DXA, QCT, etc.). To move one step further and assess the structural organization of the trabeculae, direct observation of the spine with MRI or high resolution CT scans are promising techniques, but with limited accessibility. Performing an iliac crest biopsy and carrying out an histomorphometrical analysis is an alternative but it is a rather invasive procedure. Consequently, if technically available, the quantification of the pyrrole and HP cross-link could stand as a useful marker, indicating the type of cancellous bone microarchitecture expected for a given patient.

Strengths and limitations

All measurements were made on adult human bone and we chose a skeletal site, the vertebral body, where fractures have a very high frequency (Jacobsen et al. 1992). However, as in all studies on humans, there are certain limitations. Although the analyses were carried out on 68 cylindrical samples, these important results now need to be carried out on a larger number of subjects. A second point, albeit less important, to be taken into account in the future, is the question of the length of bed-rest prior to death. Although the autopsy subjects were selected to eliminate bone or metastatic disease (Banse et al. 2001), prolonged bed-rest may have influenced the osteoid indices. However, the major emphasis of this study has been on the bulk of the collagenous matrix and microarchitecture that takes years to construct (Parfitt 1988).

Probably, the set of 3 classical parameters that we used for the assessment of osteoid (O.Th, OV/BV and OS/BS) could not account for the morphology. Indeed, the basic question is not how much new bone is formed, but rather where it is formed —i.e. more in the concavity, or more on the edge / extremity of the trabeculae. New parameters should be designed to further understand why bone remodeling may drive the structure to a thick / simple structure or rather to the preservation of a thin / more complex structure. Once again, further studies are needed in that direction.

Conclusion

This study is the first in which there is an indication of a link between the structural organization of the trabeculae and the nature of the tissue that composes these trabeculae, in terms of the cross-link stabilizing the collagen fiber.

The biochemical stability and structure of the collagen fibers may therefore be an important factor qualitatively affecting the cancellous bone turnover and hence, its final micro-architecture

Summery of the findings

1. *Patient specific information*: We observed that, after accounting for density, different patients had different bone mechanical properties. Further, the bone of a given patient was also characterized by a given structural organization of the trabeculae and by a given collagen cross-link profile. Such observations suggest a genetic control of the nature and structure of the vertebral bone tissue.
2. *Predicting bone strength*: After the density, the best predictor of bone stiffness and strength was the ratio between HP and LP cross-links. Then came some of the indices of connectivity (Star or Tb.N). While the former improved the prediction by 7 and 4% respectively, the latter only improved the prediction by 1 or 2%.
3. *Correlation between the nature and structure*: High concentrations of pyrrole cross-link and low concentrations of HP cross-link were associated with a relatively thick structure with few connections.

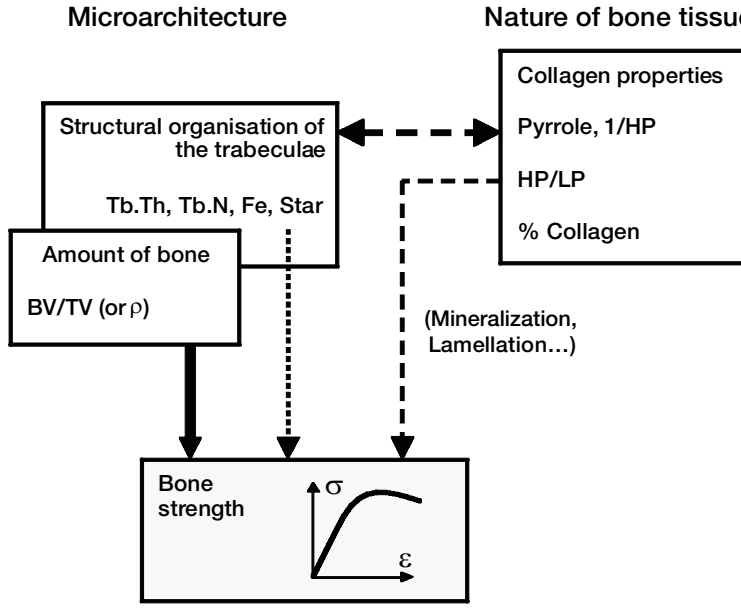

General comment

In the present work we failed, like others, to completely understand why a given sample of vertebral cancellous bone displayed a given mechanical behavior. Why?

There are at least three potential reasons for that. First, if both the microarchitecture of the trabeculae *and* the nature of bone tissue affect the strength of the sample, then showing a direct correlation between a given parameter and the mechanics becomes challenging. The higher the number of predictors, the larger the minimal sample size. The present study certainly did not include a sufficiently large number of samples and subject to support more than two predictors.

Second, the bone is a living material that continuously optimizes its microarchitecture to its functions (supporting applied forces with minimal deformation). The exact pathways of this control loop are not yet fully understood, but it is generally admitted that the basic stimulus is local strains or deformations. So, if the trabeculae of a patient are made of a tissue with (i.e.) relatively low hardness, local strains will be relatively higher. In return, this could be balanced by an adaptation of bone architecture. As both architecture and the nature of the bone are included in the control algorithm, improving our estimate of the fracture risk based on some of these parameters becomes really challenging.

Third, some important characteristics of the material were simply not investigated in the present study. Among the factors listed in Table 5, the quality or degree of the mineralization and the damage of the bone tissue probably influence bone strength and were not considered in the present work.

Addendum: pQCT as an investigation tool

Introduction

Density

There is an increasing interest for non-invasive investigations on cancellous bone. This holds true for the clinical and for laboratory investigations. Nowadays, the bone mineral density (BMD) at almost all skeletal sites (hand, wrist, hip, spine……) is readily accessible in vivo (Genant et al. 1996).

Basically these tools measure a physical property of bone: its apparent density. If one takes 1 cubic centimeter of bone (be it cortical or cancellous bone), removes all the non-bone material (fat, marrow, vessels), he can measure the amount of bone present in this sample. The amount of bone can be measured in different ways. The sample can be weighed when wet (wet apparent density, g/cm³), but this technique depends on the method used to remove the marrow without drying the bone tissue (Carter and Hayes 1977). Alternatively, the sample can be dried (Hansson et al. 1987) or freeze dried to remove all the water and then weight. This gives the dried apparent density (that we used in this study, g/cm³). Finally, the sample can be ashed in an oven (> 400° C) to remove water and the organic phase. This gives the ash apparent density which is the equivalent of the BMD. The term 'apparent' means that the volume to which the density measurement refers is the external volume of the sample, not the volume of bone tissue. For cancellous bone there is an excellent correlation between wet apparent density, dry apparent density, BMD and bone volume fraction (BV/TV) (Banse and Devogelaer 2001). The reason for this is quite clear. First the water content of bone tissue is quite constant (16 to 19%). Second the mineral content of bone tissue is also very stable, as the mineral accounts for 62 to 65% of the dry weight of bone tissue (Hansson et al. 1987; Galante et al. 1970; Mueller et al. 1966; Arnold 1960).

Regarding the cancellous bone, with aging or osteoporosis, the trabeculae do not demineralize. There is just less and less bone tissue: trabeculae disappear or get thinner. So, most of the above mentioned parameters (BV/TV, wet, dry and ash apparent density or BMD) are somewhat interchangeable for the cancellous bone—i.e., the higher the porosity, the lower the density.

All non-invasive density measurement tools (SXA, DXA, QCT, pQCT…) are based on the principle that when the X-ray (or photon) beam passes through the bone, its intensity is attenuated by the mineral. As mineral has a high atomic number compared to soft tissue or air, high density is associated with a high attenuation of the beam. Nevertheless, the density data collected from these tools *should always be validated and calibrated*, referring to an accurate external measurement (be it wet, dry or ash apparent density, or BV/TV).

Microarchitecture

Beside a correct measurement of density, some non-invasive tools (those that make tomographic images, MRI, HRCT, pQCT, μCT) give some access to the structural organization of the trabeculae (Genant et al. 1996). However, the basic concepts for the description of bone microarchitecture (like thickness, connectivity) have been originally designed for (and on) thin histological sections. So, like the density measured with a caliper rule and a balance is the gold standard for density, histology is the gold standard for the morphometry. 'Non-invasive' imagery machines should—ideally—be compared to a histological standard.

The pQCT

In part I, we measured the density of the 136 bone cylinders with a pQCT (for peripheral Quantitative Computed Tomography). The pQCT is an X-ray scanner based on the translation-rotation principle (Figure 26). It has a relatively small gantry (compared to the usual CT scan) allowing the assessments of small objects (< 8 cm in diameter). The major difference with clinical CT scans is that it has a smaller gantry (8 cm vs 80 cm) and rela-

Figure 26. pQCT scanner used for this study.

tively higher resolution (70µ vs 200µ). The major difference with µCT (micro CT) is that is has a larger gantry (for µCT typically ~1cm) a lower resolution (70µ vs 20µ). Most of all, the pQCT produces images (slice or tomography) where, for each pixel, the mineral density is quantitatively measured. The µCT does not have that property since each pixel is only assigned as being a bone or a non-bone pixel.

The pQCT has been widely used in the clinical field for investigation of the shape and density of the distal radius (Boonen et al. 1997). Some models have been adapted for the in-vivo investigation of small animals (rats, mice (Turner et al. 2001)…). or morphology (Pistoia et al. 2001; Jiang et al. 1998; Van Rietbergen et al. 1998). On the other hand, such tools have been used for the in vitro investigation of human cancellous bone density (Bailey et al. 1999; Ebbesen et al. 1997).

Purpose

In this study we had some access to the density and morphology using standard techniques (weigh scale or histology) and corresponding pQCT data.

Consequently, our working hypotheses were

1. The pQCT estimates of the density are highly correlated to the reference values
2. The pQCT allows a correct estimation of cancellous bone morphometry. More specifically the pQCT can enhance differences between the subject.

To our knowledge, there is no validation study on human material comparing histological sections with the pQCT morphological assessment. This has been done for µCT (Muller et al. 1996) but not for pQCT.

Material and methods

pQCT image acquisition

A pQCT Research SA+® (Stratec, Pfrorzheim, Germany) was used to scan the 136 cylinders. They were gently pushed in a appropriately sized plastic vial (internal diameter: 8.5 mm) just after extraction by the coring tool. There was no added liquid in the vial. Although most of the marrow was kept during coring (as needed for mechanical testing) some of it spontaneously flew out. Consequently some air bubbles were trapped between the wall of the plastic tube and some trabeculae or within the sample. Using the positioning software of the machine, the volume of the sample was divided from the bottom to the top in four equal parts. In the middle of each of these parts a pQCT image acquisition was done leaving four *slices* (named slice 1, 2, 3 and 4: see figure 27). The slice thickness was 300µ and the pixel size was 70µ by 70µ. To accommodate this resolution the translation of the x-ray source was very slow (1mm/sec) and each image was computed from 360 projections. In these conditions, the overall scan time of a cylinder was about 15 minutes. A daily calibration was performed to check the stability of the signal.

The images generated by the pQCT (272 images) were exported and converted to TIFF files (8 bit, 256 gray levels, cortical bone about 200) using NIH Scion Image® (Scion corp., Frederick, MD). Pixel size of the images was 70µm.

Density measurement with the pQCT

After the acquisition, the 544 images were analyzed with the built-in XCT 5.4 software of the pQCT. A large region of interest (ROI), wider than the cylinder, was chosen and automatically copied to all the images. Further processing was performed within the ROI, where each pixel had a given bone mineral density (BMD, given by the

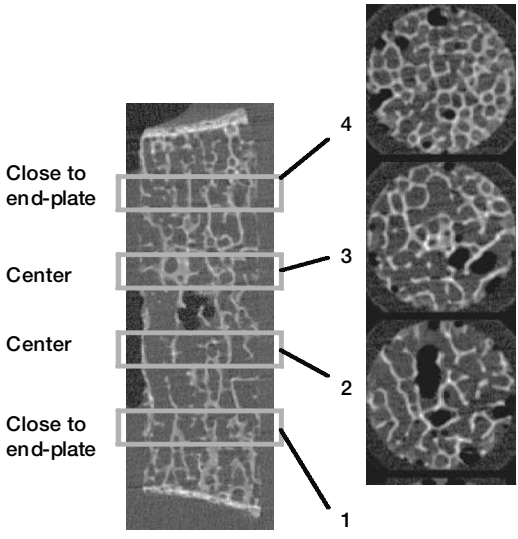

Figure 27. Typical pQCT appearance of the sample. As for the thin histological sections (see fig 11), four transverse slices were obtained from the bottom to the top of each cylinder.

machine as mgHA/cm³) inversely proportional to the attenuation of the X-ray beam within the corresponding voxel. An image segmentation (understand a selection of a sub-population of these pixels) was done using a constant threshold value of 200 mgHA/cm³. This thresholding procedure eliminates all pixels corresponding to air (value < 0 mgHA/cm³) or saline (value: 60 mgHA/cm³ on the pQCT). A previous study had shown that this was an optimal value (Banse and Devogelaer 2000) Consequently, no pixel outside the external perimeter of the cylinder was selected, and the region of interest was automatically and exactly restricted to the sample.

The bone mineral density as measured by the pQCT (pQCT BMD, mgHA/cm³) was calculated as the mean BMD of all the selected pixels multiplied by the proportion of surface that was selected by the thresholding procedure. Practically this proportion was the surface of selected pixels (mm²) divided by the cross-sectional area of the sample (52.8 mm²).

Apparent density

We measured the physical or true apparent density on the 68 samples from one side that have been used for the biochemical analysis (see part III). The end-plates were removed to only consider the volume that was mechanically tested and assessed by pQCT. Bone marrow was removed with a water jet and the samples were defatted. All samples were then freeze-dried, and weighed to give the dry weight (W_D, g). Their height (without end-plates) was measured twice with a caliper (Mitotoyo, UK). The volume of the cylinders was calculated as the product of their height by their cross-sectional area (constant 52.8 mm²). The apparent density (ρ_{app}, g/cm³) was obtained using the formula: W_D / volume.

Architectural parameters

For each of the 272 Von Kossa thin sections described in part II, we analyzed the corresponding pQCT image. This was done on the same computer with the same image analysis software, running the same macro. Only the segmentation of the original image was different: for the pQCT, we used a 'whiter than 85' constant threshold, while for the histological images it was a 'darker than 100' threshold.

Data processing and statistical analysis

Density values (ρ_{app}) were compared to the mean of the four pQCT BMD values of a given cylinder using linear regression.

To estimate the relative accuracy or limitations of the pQCT images to provide a correct morphometrical assessment of a given cylinder, results coming from the four slices of each of them were grouped in a single mean value (68 x 2 average values for the 68 cylinders). Linear regression analysis was then used to estimate the correlation between pQCT and histology.

We also compared the capacity of the two types of investigations to point out differences among subjects using η^2 values. This procedure is described in part II.

Results

Measuring density

The pQCT gave an excellent estimation of the apparent density of the cylinders (Figure 28).

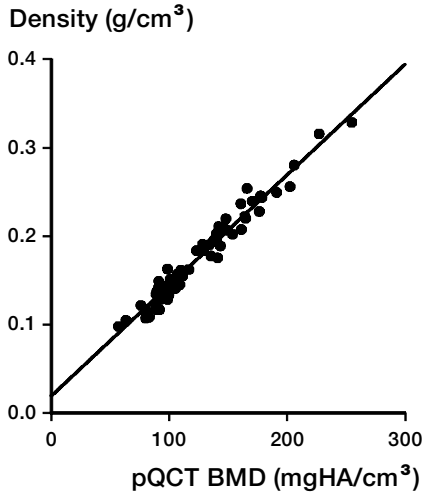

Figure 28. The pQCT gave a very good estimate of density.

Measuring morphometry

On gross examination the pQCT images demonstrated similar morphological characteristics as seen on corresponding histological thin sections (Figure 29).

The BV/TV values obtained with the pQCT were two times higher than on the thin sections (16% vs 8%). On analyzing the pQCT images, the trabeculae appeared two times thicker than their histological control (Tb.Th 161 μm vs 83 μm). The Tb.N was not over-estimated by the pQCT and Tb.Sp slightly underestimated (the difference, 100 μm corresponds to the increase in thickness of the trabeculae). For the strut analysis, the mean TSL values were identical but the pQCT detected fewer nodes and free-ends than the histology.

The pQCT values of BV/TV, Tb.N, Tb.Sp correlated very well with the histological values ($r > 0.93$). The estimation of the mean Tb.Th of a given cylinder was fairly good ($r = 0.83$) knowing that the pixel size was 70 μm and the mean Tb.Th on histology was 84μm (Figure 30). In the strut analysis (Figure 31), the correlation for TSL was excellent ($r = 0.94$). On segmenting the skeleton, the pQCT scanner was less efficient to detect the Fe ($r = 0.79$) than the nodes ($r = 0.86$). The connectivity was better estimated by the pQCT when measuring the Star ($r = 0.91$, Figure 32) than the Nd/Fe ratio ($r = 0.81$).

Discussion

Density

The pQCT BMD was an excellent predictor of the true apparent density.

The physical properties of our samples are consistent with previously published results. We found a mean value 0.175 g/cm³ for the apparent density while Galante et al. (1970) found 0.19 g/cm³ and Hansson et al. (1980) 0.15 g/cm³, both of them using the weight of dry bone to estimate the apparent density.

Knowing a-priori the apparent density of a sample is most useful for biomechanical investigations (Keaveny et al. 1994) or when the sample itself has to be used for another purpose than density measurement (Bailey et al. 1999). However, for such non-destructive investigations to be useful, it should relieve the investigators from any processing of the sample before the measurement. First, if the marrow has to be removed and the sample to be processed before scanning, then why not directly weigh it? Second, for many biomechanical protocols, the bone marrow has to be retained in situ (Carter and Hayes 1977) (dynamic tests) and defatting is known to affect the mechanical properties (Linde and Sorensen 1993). Third, a non-destructive assessment of the density should be a fast procedure, not only to save time but also to avoid decay of the sample, especially if marrow is kept in place. With a scan time of less than 15 minutes, the cylinder was just thawed but still cold when going back to the deep-freezer. Consequently, the protocol was realistic, respecting the limitations of a density measurement preliminary to biomechanical tests.

However, there were two sources of random errors in our pQCT acquisition protocol. The amount of bone varies from the bottom to the top of the specimen (Banse et al. 2001). As the sample is not homogeneous, each cubic millimeter of the specimen should be analyzed by the pQCT to get as close as possible to the reference measurement that takes the whole specimen into account. The pQCT acquisition was limited to 4 slices, each 0.3mm thick and, consequently, we just scanned 2.5 ± 0.5 % of its total volume. This constitutes a first source of random error. Another source of inaccuracy was the variability of the

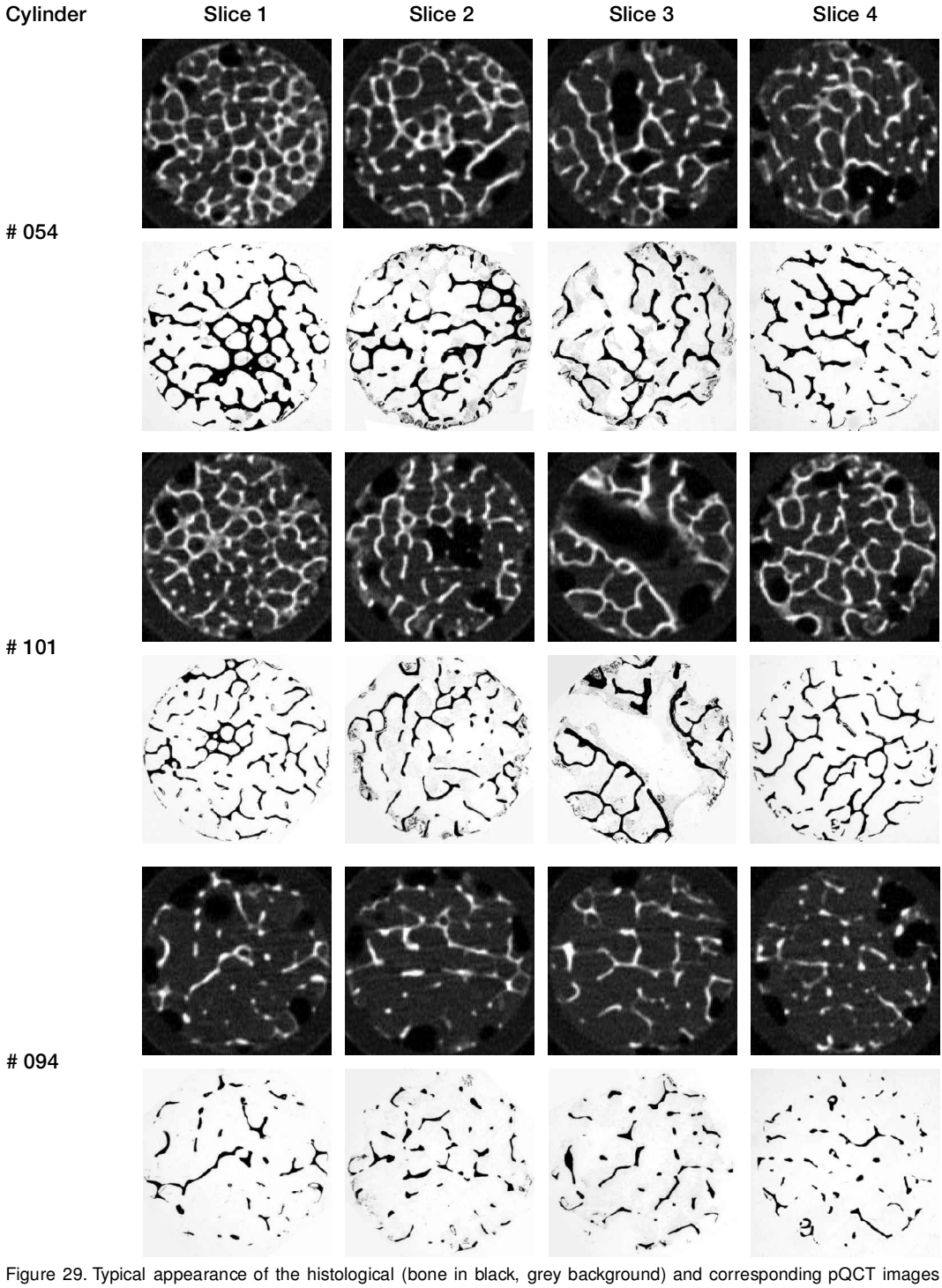

Figure 29. Typical appearance of the histological (bone in black, grey background) and corresponding pQCT images (bone in white, background black). Three cylindrical samples are shown. From the left to the right: Cylinder # 054 has a high density (BV/TV = 15.5%), relatively thick trabeculae, well connected. Cylinder # 101 has a medium density (BV/TV = 10.6%); note, in slice 3, that both techniques show the nice vascular channel crossing the cylinder. Cylinder # 094 illustrates a low density sample (BV/TV 5.4%) with a few very thin and disconnected trabeculae. (Modified from Banse et al. 2002b, with permission from Elsevier Science).

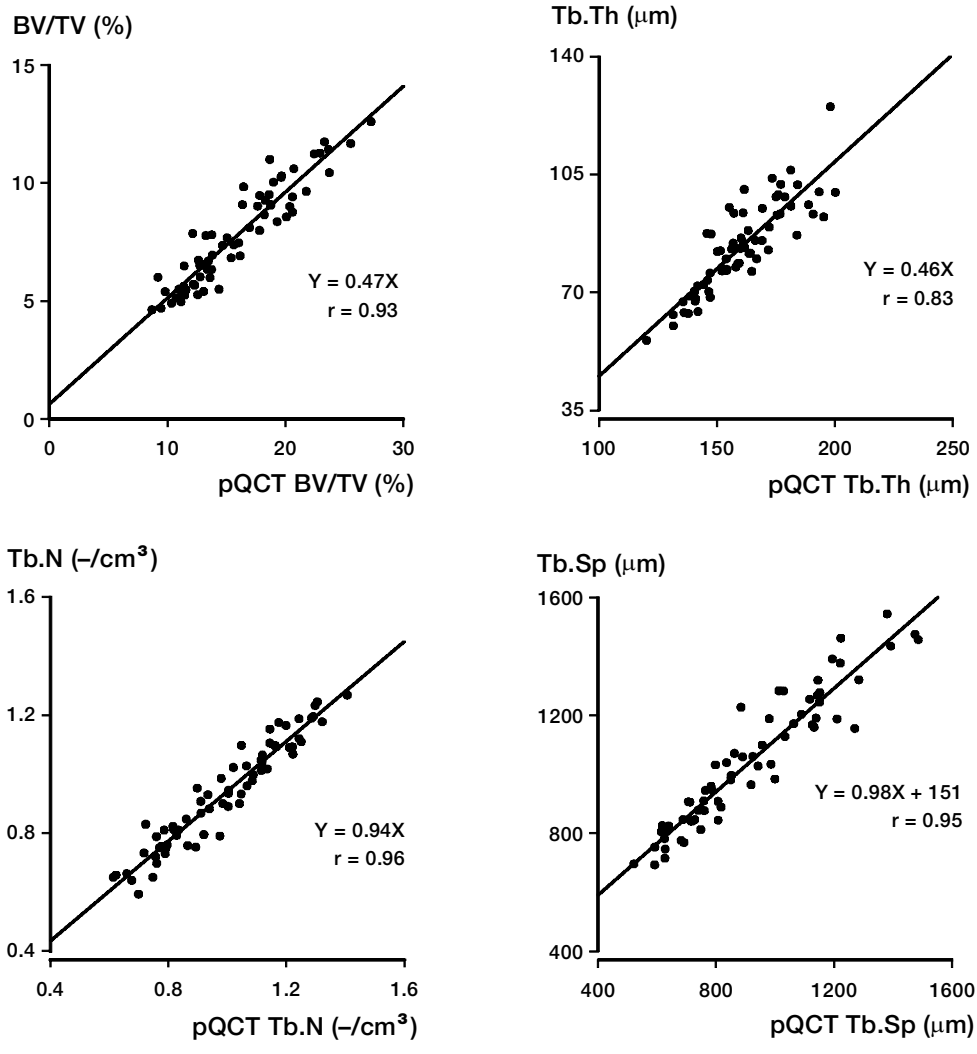

Figure 30. Diagram showing the correlation between the 'classical' morphometrical parameters obtained from histology and pQCT. They are all based on the detection of bone surfaces and perimeter. Even if the pQCT detects a bone surface twice as big as the histological control, the correlation is excellent.

nature of the medium surrounding the trabeculae. Air bubbles could certainly represent a problem, but also the more or less 'fatty' nature of the marrow (McBroom et al. 1985). The pQCT machine itself is calibrated in such a way that (when expressed in BMD value) the air value is –282 mgHA/cm³, the fat value is 0 mgHA/cm³ and the saline value (or the red marrow) is 50 to 60 mgHA/cm³. If all the pixels are considered, the mean BMD of a sample in air (with 15% of bone and 85% of air) is not the same as that of the same sample in water (15% bone and 85% water). The only way to eliminate this second source of inaccuracy is to remove everything (air and marrow) and to replace it by another homogeneous 'medium' (usually air, water or saline) (Jiang et al. 1998; Ebbesen et al. 1997). Fortunately, the pQCT has the capacity to eliminate most of this error with the image segmentation. A preliminary study (Banse and Devogelaer 2000) indicated that the optimal threshold was 200 mgHA/cm³. The thresholding procedure selected a surface equivalent to twice the bone volume fraction (Figure 30). For instance, when the bone

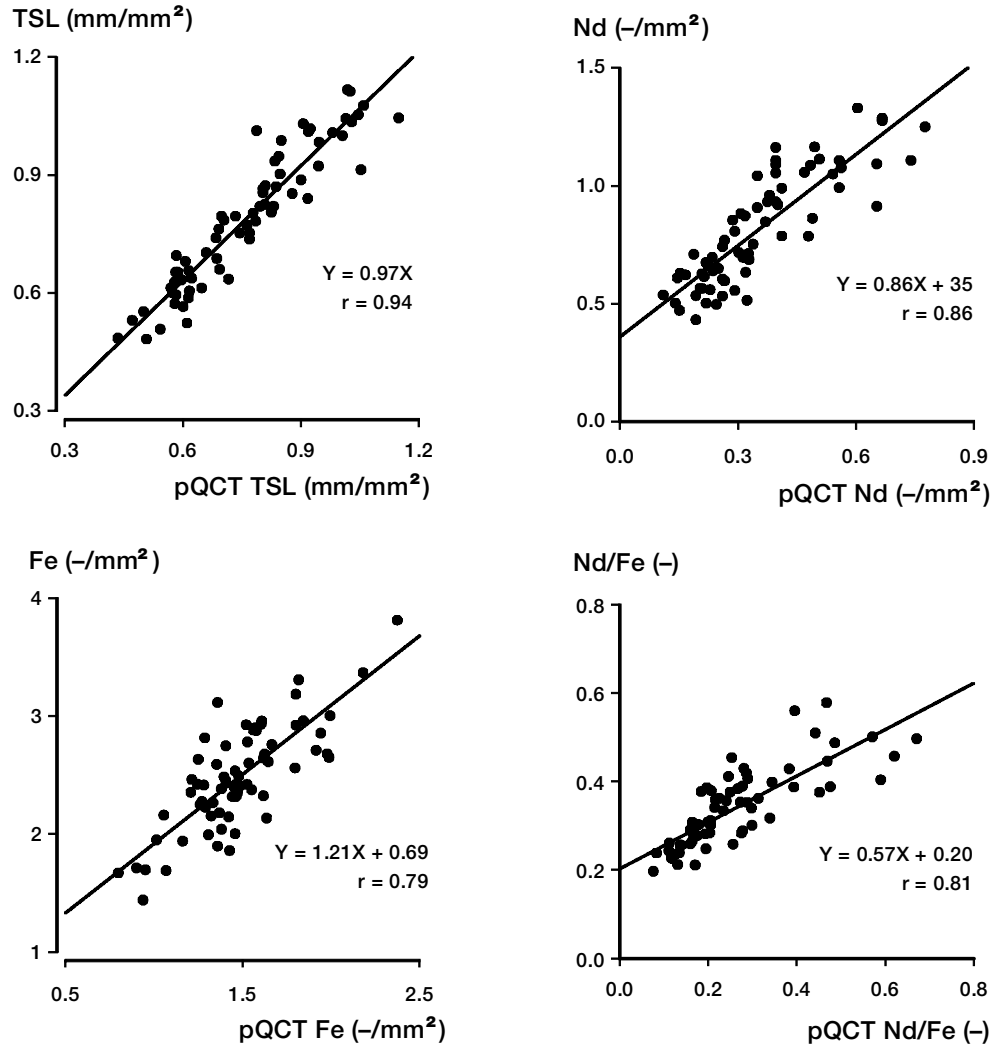

Figure 31. Performing a strut analysis on the pQCT images was also efficient. The total strut length (TSL) was identical on both types of image and the correlation was excellent. Detection of the Fe seemed less efficient with the pQCT.

volume fraction was 10%, the pQCT selected 20% of the pixels, thus eliminating the majority of the 'non bone pixels'. This thresholding procedure probably reduced the scattering effect or random error due to the marrow and air bubbles.

For the prediction of apparent ash density of 95 iliac crest samples (with bone marrow in place but no air bubbles) Ebbesen et al. (1997)obtained an identical correlation coefficient (r = 0.98).

These data validate the conversion of pQCT BMD values to apparent density as we did in Part I.

Morphometry

Practically, the pQCT gave a correct image of the vertebral bone morphology (Figure 29) and gave almost the same amount of information as the histology (Figure 30, 31 and 32). This is somewhat puzzling when comparing the volume of interest that was considered to give its gray value to each pixel. This volume is called voxel by the radiologists, and corresponds to the pixel size x the slice thickness. Basically this gray level tells us if we need to consider that precise volume as being bone or marrow. The voxel size with the pQCT was 1,470,000 μm³ (70 × 70 × 300 μm) and 500 μm³

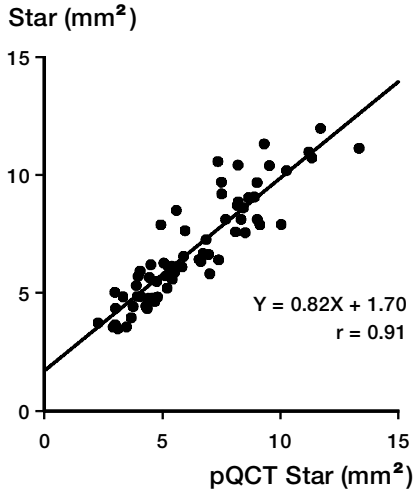

Figure 32. The pQCT correctly identified the samples with high Star, or those with relatively low connectivity.

(10 × 10 × 5 μm) on the thin histological sections.

Three technical details have to be mentioned. First we did not make any effort to match the true BV/TV with the amount of selected pixels in the pQCT images. Our idea was that we preferred to overestimate BV/TV than to loose structural elements. Forcing the pQCT BV/TV to fit the true histological value (8%) has a price: a lot of structural elements are lost (Kothari et al. 1998; Ito et al. 1998). Secondly, the number of images (four) used for the assessment of a given cylinder is identical with both type of images. Morphological parameters from the pQCT were not extracted from a volumetric acquisition (Laib and Ruegsegger 1999; Muller et al. 1998). This means that the same surface of bone (in the images) is used to extract morphological parameters (Figure 29). Third, both type of images (Histological and pQCT) were treated by the same macro, with the same software and on the same computer, as to increase the comparability of the data.

Studies directly comparing scanner images with histological sections are scarce. Muller et al. (1998) obtained comparable correlation coefficients for the standard morphometrical parameters but their voxel size was 500 times smaller (2,744 μm³, 14 x 14 x 14 μm3) than the one used in this study. Classical morphometrical parameters were measured with a μCT on 63 *iliac crest* biopsies and yielded an almost identical correlation coefficient as found in this study (they reported r for BV/TV = 0.93, Tb.Th = 0.84, Tb.Sp = 0.91). Kuhn et al. (1990) obtained similar results but their threshold value was adapted to account for putative variation in the tissue density.

The only work comparing high resolution CT scanner and histo-morphometry *on vertebral bone* was carried out with samples coming from ewe (Mitton et al. 1998). In this species the BV/TV is much higher than in humans and their resolution was lower than ours (voxel size of 3,375,000 μm³ or 150 × 150 × 150 μm). Consequently, they observed slightly lower correlation coefficient. However, the consistent point is that when running a strut analysis they also observed a good correlation with the TSL (r = 0.83) and experienced more difficulties to identify the Fe (r = 0.52).

The good correlations we observed between histology and pQCT may be linked to the structure of vertebral cancellous bone. The true BV/TV (measured by histology) is very low in the human vertebral body (90% of the total volume is occupied by marrow) and the space between trabeculae is pretty high (about 0.5 to 1.5 mm) allowing a correct identification of the trabeculae by pQCT.

With the simple threshold algorithm used for pQCT image segmentation a pixel was accounted as being bone, even when only a part of the voxel (50%) was truly occupied by bone. This explains the overestimation of the Tb.Th with low-resolution scanners as well as the two times higher BV/TV we observed. With the pQCT, every trabecula was considerably 'thickened' by the scanner (Figure 29 and 30B) but, provided that each feature (trabeculae) is sufficiently separated from the others, this phenomenon does not seem to prevent a correct morphometrical assessment.

On the pQCT images the identification of the multiple points or Nd from the skeleton was fairly good (r = 0.86) but the detection of the free ends (r = 0.79) seemed to be more problematic. This may be related to technical reasons. Slices were so thick (300 μm) with the pQCT that a bony feature disconnected on the histological image (5 μm thick) appeared as connected on the pQCT image. Considering a perforated trabecular plate (a frequent event), the histological image will show a disconnection, while a few microns below and above, the structure is actually connected with the rest

Table 9. η^2 **value for detection of between subject differences with pQCT and histology**

	Technique used	
Parameter	pQCT	Histology
Tb.Th* (µm)	0.64 [c]	0.73 [c]
Tb.N* (–/mm^2)	0.62 [c]	0.63 [c]
Tb.Sp* (µm)	0.55 [c]	0.62 [c]
TSL* (mm/mm^2)	0.61 [c]	0.58 [c]
Nd* (–/mm^2)	0.15	0.49 [c]
Fe (–/mm^2)	0.67 [c]	0.70 [c]
Nd/Fe* (–)	0.21	0.34 [b]
Star* (mm^2)	0.39 [c]	0.54 [c]

η^2 value is an estimation of the part of the overall variance that is due to differences between the subjects. P-value is for test that the effect of the considered variable = 0.
Key: [a] $p < 0.05$, [b] $p < 0.01$, [c] $p < 0.0001$. * indicates that the BV/TV has been introduced as covariable.

of the network. We do not know which method gives mechanically relevant measurements. Technically, the pruning algorithm certainly influenced the number of Fe. For the analysis of both pQCT and histological images we removed all parasiting branches with a length less than the Tb.Th. However, while the length of the network was identical for both types of images, the Tb.Th was 84 µm on histology and 163 µm on pQCT images. Consequently we probably removed more parasiting branches with the pQCT. As such element is composed of one Nd and one Fe, this explains why we have less Nd and less Fe on the pQCT images.

Detection of differences between patients

A systematic analysis of the morphometrical parameters allowed us to pick up those that have the best ability to differentiate patients. Considering Table 9, it seems clear that Fe and Tb.Th are the most sensitive parameters. Interestingly, this holds true for both pQCT and histological analysis. For the detection of between-subjects differences, the pQCT is slightly less efficient than the histological analysis (η^2 values were lower for the pQCT). However, the estimated marginal means correlated very well in both methods (except for the nodes and node related parameters). When a clear patient specific structural pattern was detectable by the histology, the pQCT picked up the same information (i.e. this patient has more Fe, smaller trabeculae, higher Star….). The only parameter for which the pQCT lost the patient specific information was the Nd.

Confirmation

Overall, we consider the pQCT morphological information as reliable. In parts II and IV we used microarchitectural parameters determined with histology on 68 samples. What if we use the pQCT microarchitectural data trying to improve the prediction of the mechanical behavior (with n = 136) ? None of the pQCT morphometrical parameters significantly improved the prediction of bone stiffness and strength. Maybe the Tb.N slightly improved the prediction of bone strength (partial correlation coefficient r = 0.21, p = 0.015). However such an improvement was marginal.

In part IV the cross-link profile of a given cylinder was compared to the microarchitecture of the paired controlateral one. We assumed that the morphometry would be identical on both left and right sides. On comparing the pQCT data from both histology and biochemistry subgroups we obtained good correlation (r values between 0.75 and 0.9). Secondly, we can explore if the cross-link content of a cylinder is correlated with the pQCT microarchitecture of that same cylinder. Doing that, we clearly confirmed with the pQCT the observations reported in part IV: high pyrrole—or low HP—mean high pQCT Tb.Th (r = 0.59 and r = –0.50) and less pQCT Fe (r = –0.45 and r = 0.34).

pQCT as investigation tool

Overall, these data indicate that the pQCT is an excellent investigation tool to measure both bone density and microarchitecture. This was true even in poor conditions (with air bubbles, marrow and few slices).

Acknowledgements

This work was made possible thanks to two consecutive grants form the National Fund for Scientific Research (FNRS, Belgium). These grants allowed me to work during four years as a research fellow in the Université Catholique de Louvain (UCL).

My special gratitude goes to Professor Christian Delloye, my principal supervisor, who introduced me, ten years ago, to the field of orthopedic research. His enthusiastic support, continuous interest, stimulating criticism and kind friendship helped me every day from the very beginning of the thesis. I am deeply indebted to Professor Everard Munting who sensitized me to the problem of spinal fracture and initiated this work. Professor Jean Pierre Devogelaer communicated his expertise in the field of osteoporosis and densitometry. The pQCT study was performed in his laboratory. Pr. Rombouts provided also an essential support to this thesis.

The present work certainly results from the collaboration between different Universities. Marc Grynpas, Professor at the University of Toronto guided and directly supervised this work. His broad knowledge of the bone material and bone biology was invaluable in the achievement of the present work. I thank him for welcoming me repeatedly in his laboratory. Professor Allen Bailey from the University of Bristol offered me the opportunity to explore some aspects of the bone collagen matrix. All the cross-links analyses were performed in his laboratory. The thoughtful discussions with both these scientists will remain as extraordinary moments for me. I am also deeply indebted to Professor John Van Tomme and Luc Rabet who gave me access to all the facilities at the civil engineering department of the Royal Military Academy of Brussels.

A special thank goes to Claudette Benoît, Pascale Smitz, Aime Decoster, Trevor Sims and Mircea Dimitriu for their skillful technical support.

References

Alexiades M M, Boachie-Adjei O, Vigorita V J. Histomorphometric analysis of vertebral and iliac crest bone samples. A correlated study. Spine 1990; 15 (4): 286-8.

Arnold J S. Quantitation of mineralization of bone as an organ and tissue in osteoporosis. Clin Orthop 1960; 17: 167-75.

Ashman R B, Rho J Y. Elastic modulus of trabecular bone material. J Biomech 1988; 21 (3): 177-81.

Bailey A J, Sims T J, Ebbesen E N, Mansell J P, Thomsen J S, Mosekilde L. Age-related changes in the biochemical properties of human cancellous bone collagen: relationship to bone strength. Calcif Tissue Int 1999; 65: 203-10.

Bailey A J, Wotton S F, Sims T J, Thompson P W. Post-translational modifications in the collagen of human osteoporotic femoral head. Biochem Biophys Res Commun 1992; 185 (3): 801-5.

Bank R A, Robins S P, Wijmenga C, Breslau-Siderius L J, Bardoel A F, van der Sluijs H A, Pruijs H E, TeKoppele J M. Defective collagen crosslinking in bone, but not in ligament or cartilage, in Bruck syndrome: indications for a bone-specific telopeptide lysyl hydroxylase on chromosome 17. Proc Natl Acad Sci U S A 1999; 96 (3): 1054-8.

Banse X, Devogelaer J P. Validation of pQCT for human vertebral bone samples density measurement. Osteoporosis Int 2000; 11 (suppl. 3), S39.

Banse X, Devogelaer J P. Does the pQCT ignore the tissue density ? J Clin Densitom 2002; (In press)

Banse X, Devogelaer J P, Munting E, Delloye C, Cornu O, Grynpas M D. Inhomogeneity of human vertebral cancellous bone. Systematic density and structure patterns inside the vertebral body. Bone 2001; 28 (5): 563-71.

Banse X, Devogelaer J P, Grynpas M. Patient specific microarchitecture of the vertebral cancellous bone: A pQCT and histological study. Bone 2002a; (In press)

Banse X, Lafosse A, Grynpas M, Bailey A J. The cross-link profile of bone collagen correlates with the structural organization of the trabeculae. Bone 2002b; (In press).

Banse X, Sims T J, Bailey A J. Mechanical properties of adult vertebral cancellous bone: Correlation with collagen intermolecular cross-links. J Bone Miner Res 2002c; (In press).

Batge B, Diebold J, Stein H, Bodo M, Muller P K. Compositional analysis of the collagenous bone matrix. A study on adult normal and osteopenic bone tissue. Eur J Clin Invest 1992; 22 (12): 805-12.

Bell G H, Dunbar O, Beck J S, Gibb A. Variations in strength of vertebrae with age and their relation to osteoporosis. Calcif Tissue Res 1967; 1 (1): 75-86.

Boonen S, Cheng X G, Nijs J, Nicholson P H, Verbeke G, Lesaffre E, Aerssens J, Dequeker J. Factors associated with cortical and trabecular bone loss as quantified by peripheral computed tomography (pQCT) at the ultradistal radius in aging women. Calcif Tissue Int 1997; 60 (2): 164-70.

Boskey A L, Wright T M, Blank R D. Collagen and bone strength. J Bone Miner Res 1999; 14 (3): 330-5.

Brady J D, Robins S P. Structural characterization of pyrrolic cross-links in collagen using a biotinylated Ehrlich's reagent. J Biol Chem 2001; 276 (22): 18812-8.

Burr D B, Forwood M R, Fyhrie D P, Martin R B, Schaffler M B, Turner C H. Bone microdamage and skeletal fragility in osteoporotic and stress fractures . J Bone Miner Res 1997; 12 (1): 6-15.

Carter D R, Hayes W C. The compressive behavior of bone as a two-phase porous structure. J Bone Joint Surg [Am] 1977; 59 (7): 954-62.

Chappard D, Legrand E, Pascaretti C, Basle M F, Audran M. Comparison of eight histomorphometric methods for measuring trabecular bone architecture by image analysis on histological sections. Microsc Res Tech 1999; 45: 303-12.

Compston J E. Connectivity of cancellous bone: assessment and mechanical implications [editorial]. Bone 1994; 15: 463-6.

Compston J E, Mellish R W, Croucher P, Newcombe R, Garrahan N J. Structural mechanisms of trabecular bone loss in man. Bone Miner 1989; 6: 339-50.

Compston J E, Mellish R W, Garrahan N J. Age-related changes in iliac crest trabecular microanatomic bone structure in man. Bone 1987; 8: 289-92.

Consensus development conference. Consensus development conference: diagnosis, prophylaxis, and treatment of osteoporosis. Am J Med 1993; 94 (6): 646-50.

Cooper C, Atkinson E J, Jacobsen S J, O'Fallon W M, Melton L J. Population-based study of survival after osteoporotic fractures. Am J Epidemiol 1993; 137 (9): 1001-5.

Croucher P I, Garrahan N J, Compston J E. Assessment of cancellous bone structure: comparison of strut analysis, trabecular bone pattern factor, and marrow space star volume. J Bone Miner Res 1996; 11 (7): 955-61.

Currey J D. Mechanical adaptations of bones Princeton University press, Princeton (N.J.) 1984.

Day J S, Ding M, Odgaard A, Sumner D R, Hvid I, Weinans H. Parallel plate model for trabecular bone exhibits volume fraction-dependent bias. Bone 2000; 27 (5): 715-20.

Dempster D W. The contribution of trabecular architecture to cancellous bone quality [editorial]. J Bone Miner Res 2000; 15 20-3.

Dequeker J. Assessment of quality of bone in osteoporosis--BIOMED I: fundamental study of relevant bone. Clin Rheumatol 1994; 13 (suppl. 1): 7-12.

Ding M. Age variations in the properties of human tibial trabecular bone and cartilage. Acta Orthop Scand 2000; suppl. 292: 1-45.

Ebbesen E N, Thomsen J S, Mosekilde L. Nondestructive determination of iliac crest cancellous bone strength by pQCT. Bone 1997; 21: 535-40.

Eyre D R. Biochemical basis of collagen metabolites as bone turnover markers. In: Principles of bone biology (Eds.J P Bilezikian, L G Raisz, and G A Rodan). Academic Press. San Diego: 1996; 11: 143-54.

Eyre D R, Dickson I R, Van-Ness K. Collagen cross-linking in human bone and articular cartilage. Age-related changes in the content of mature hydroxypyridinium residues. Biochem J 1988; 252 (2): 495-500.

Frost H M. Dynamics of bone remodeling. In: Bone Biodynamics (Ed. H M Frost). Little & Brown. Boston: 1964; 18: 315-34.

Galante J, Rostoker W, Ray R D. Physical properties of trabecular bone. Calcif Tissue Res 1970; 5 (3): 236-46.

Genant H K, Engelke K, Fuerst T, Gluer C C, Grampp S, Harris S T, Jergas M, Lang T, Lu Y, Majumdar S, Mathur A, Takada M. Noninvasive assessment of bone mineral and structure: state of the art. J Bone Miner Res 1996; 11: 707-30.

Gibson L J. The mechanical behaviour of cancellous bone. J Biomech 1985; 18 (5): 317-28.

Glimcher M J, Krane S M. Organization and structure of bone, and the mechanism of calcifiction. In: A treatise on collagen (Eds.B S Gould and G N Ramachandran). Academic Press. London and New York: 1968; 2: 68-241.

Gluer C C, Cummings S R, Bauer D C, Stone K, Pressman A, Mathur A, Genant H K. Osteoporosis: association of recent fractures with quantitative US findings. Radiology 1996; 199 (3): 725-32.

Gordon C L, Lang T F, Augat P, Genant H K. Image-based assessment of spinal trabecular bone structure from high-resolution CT images. Osteoporos Int 1998; 8: 317-25.

Gordon C L, Webber C E, Adachi J D, Christoforou N. In vivo assessment of trabecular bone structure at the distal radius from high-resolution computed tomography images. Phys Med Biol 1996; 41: 495-508.

Goulet R W, Goldstein S A, Ciarelli M J, Kuhn J L, Brown M B, Feldkamp L A. The relationship between the structural and orthogonal compressive properties of trabecular bone. J Biomech 1994; 27 (4): 375-89.

Grant R A. Estimation of hydroxyproline by the AutoAnalyzer. J Clin Pathol 1965; 18 (5): 686.

Grynpas M D. Age and disease-related changes in the mineral of bone. Calcif Tissue Int 1993; 53 (Suppl. 1): S57-S64

Hahn M, Vogel M, Pompesius-Kempa M, Delling G. Trabecular bone pattern factor--a new parameter for simple quantification of bone microarchitecture. Bone 1992; 13 (4): 327-30.

Hanson D A, Eyre D R. Molecular site specificity of pyridinoline and pyrrole cross-links in type I collagen of human bone. J Biol Chem 1996; 271 (43): 26508-16.

Hansson T, Roos B, Nachemson A. The bone mineral content and ultimate compressive strength of lumbar vertebrae. Spine 1980; 5 (1): 46-55.

Hansson T H, Keller T S, Panjabi M M. A study of the compressive properties of lumbar vertebral trabeculae: effects of tissue characteristics. Spine 1987; 12: 56-62.

Heaney R P. The natural history of vertebral osteoporosis. Is low bone mass an epiphenomenon? Bone 1992; 13 Suppl 2 S23-S26

Heaney R P. Is there a role for bone quality in fragility fractures? Calcif Tissue Int 1993; 53 (Suppl. 1): S3-S5

Hildebrand T, Laib A, Muller R, Dequeker J, Ruegsegger P. Direct three-dimensional morphometric analysis of human cancellous bone: microstructural data from spine, femur, iliac crest, and calcaneus. J Bone Miner Res 1999; 14 (7): 1167-74.

Hou F J, Lang S M, Hoshaw S J, Reimann D A, Fyhrie D P. Human vertebral body apparent and hard tissue stiffness. J Biomech 1998; 31 (11): 1009-15.

Ito M, Nakamura T, Matsumoto T, Tsurusaki K, Hayashi K. Analysis of trabecular microarchitecture of human iliac bone using microcomputed tomography in patients with hip arthrosis with or without vertebral fracture. Bone 1998; 23: 163-9.

Jacobsen S J, Cooper C, Gottlieb M S, Goldberg J, Yahnke D P, Melton L J. Hospitalization with vertebral fracture among the aged: a national population-based study, 1986-1989. Epidemiology 1992; 3 (6): 515-8.

Jiang Y, Zhao J, Augat P, Ouyang X, Lu Y, Majumdar S, Genant H K. Trabecular bone mineral and calculated structure of human bone specimens scanned by peripheral quantitative computed tomography: relation to biomechanical properties. J Bone Miner Res 1998; 13 (11): 1783-90.

Kabel J, Odgaard A, Van Rietbergen B, Huiskes R. Connectivity and the elastic properties of cancellous bone [see comments]. Bone 1999; 24 115-20.

Kabel J, Van Rietbergen B, Odgaard A, Huiskes R. Constitutive relationships of fabric, density, and elastic properties in cancellous bone architecture. Bone 1999; 25 (4): 481-6.

Keaveny T M, Guo X E, Wachtel E F, McMahon T A, Hayes W C. Trabecular bone exhibits fully linear elastic behavior and yields at low strains. J Biomech 1994; 27 (9): 1127-36.

Keaveny T M, Pinilla T P, Crawford R P, Kopperdahl D L, Lou A. Systematic and random errors in compression testing of trabecular bone. J Orthop Res 1997; 15 (1): 101-10.

Keaveny T M, Wachtel E F, Kopperdahl D L. Mechanical behavior of human trabecular bone after overloading. J Orthop Res 1999; 17 (3): 346-53.

Kimmel D B, Recker R R, Gallagher J C, Vaswani A S, Aloia J F. A comparison of iliac bone histomorphometric data in post-menopausal osteoporotic and normal subjects. Bone Miner 1990; 11 (2): 217-35.

Kleerekoper M, Villanueva A R, Stanciu J, Rao D S, Parfitt A M. The role of three-dimensional trabecular microstructure in the pathogenesis of vertebral compression fractures. Calcif Tissue Int 1985; 37 (6): 594-7.

Knott L, Bailey A J. Collagen cross-links in mineralizing tissues: a review of their chemistry, function, and clinical relevance. Bone 1998; 22 (3): 181-7.

Knott L, Tarlton J F, Bailey A J. Chemistry of collagen cross-linking: biochemical changes in collagen during the partial mineralization of turkey leg tendon. Biochem J 1997; 322 (Pt 2): 535-42.

Knott L, Whitehead C C, Fleming R H, Bailey A J. Biochemical changes in the collagenous matrix of osteoporotic avian bone. Biochem J 1995; 310 (Pt 3): 1045-51.

Kopperdahl D L, Keaveny T M. Yield strain behavior of trabecular bone. J Biomech 1998; 31 (7): 601-8.

Kopperdahl D L, Roberts A D, Keaveny T M. Localized damage in vertebral bone is most detrimental in regions of high strain energy density. J Biomech Eng 1999; 121: 622-8.

Kothari M, Keaveny T M, Lin J C, Newitt D C, Genant H K, Majumdar S. Impact of spatial resolution on the prediction of trabecular architecture parameters. Bone 1998; 22 (5): 437-43.

Kuhn J L, Goldstein S A, Feldkamp L A, Goulet R W, Jesion G. Evaluation of a microcomputed tomography system to study trabecular bone structure. J Orthop Res 1990; 8 (6): 833-42.

Kuypers R, Tyler M, Kurth L B, Jenkins I D, Horgan D J. Identification of the loci of the collagen-associated Ehrlich chromogen in type I collagen confirms its role as a trivalent cross-link. Biochem J 1992; 283 (Pt 1): 129-36.

Laib A, Ruegsegger P. Calibration of trabecular bone structure measurements of in vivo three-dimensional peripheral quantitative computed tomography with 28-microm-resolution microcomputed tomography. Bone 1999; 24 (1): 35-9.

Legrand E, Chappard D, Pascaretti C, Duquenne M, Krebs S, Rohmer V, Basle M F, Audran M. Trabecular bone microarchitecture, bone mineral density, and vertebral fractures in male osteoporosis. J Bone Miner Res 2000; 15: 13-9.

Li B, Aspden R M. Composition and mechanical properties of cancellous bone from the femoral head of patients with osteoporosis or osteoarthritis. J Bone Miner Res 1997; 12 (4): 641-51.

Lindahl O. Mechanical properties of dried defatted spongy bone. Acta Orthop Scand 1976; 47 (1): 11-9.

Linde F, Hvid I, Madsen F. The effect of specimen geometry on the mechanical behaviour of trabecular bone specimens. J Biomech 1992; 25 (4): 359-68.

Linde F, Sorensen H C. The effect of different storage methods on the mechanical properties of trabecular bone. J Biomech 1993; 26 (10): 1249-52.

Majumdar S, Kothari M, Augat P, Newitt D C, Link T M, Lin J C, Lang T, Lu Y, Genant H K. High-resolution magnetic resonance imaging: three-dimensional trabecular bone architecture and biomechanical properties. Bone 1998; 22 (5): 445-54.

Mansell J P, Bailey A J. Abnormal cancellous bone collagen metabolism in osteoarthritis. J Clin Invest 1998; 101 (8): 1596-603.

Marks S C, Hermey D C. The structure and development of bone. In: Principles of bone biology (Eds.J P Bilezikian, L G Raisz, and G A Rodan). Academic Press. San Diego: 2001; 1: 3-14.

Marotti G. A new theory of bone lamellation. Calcif Tissue Int 1993; 53 (Suppl 1): S47-S55

Martin R B, Burr D B. A hypothetical mechanism for the stimulation of osteonal remodelling by fatigue damage. J Biomech 1982; 15 (3): 137-9.

McBroom R J, Hayes W C, Edwards W T, Goldberg R P, White A A. Prediction of vertebral body compressive fracture using quantitative computed tomography. J Bone Joint Surg [Am] 1985; 67 (8): 1206-14.

McCalden R W, McGeough J A, Court B C. Age-related changes in the compressive strength of cancellous bone. The relative importance of changes in density and trabecular architecture. J Bone Joint Surg [Am] 1997; 79 (3): 421-7.

Mellish R W, Ferguson-Pell M W, Cochran G V, Lindsay R, Dempster D W. A new manual method for assessing two-dimensional cancellous bone structure: comparison between iliac crest and lumbar vertebra. J Bone Miner Res 1991; 6: 689-96.

Melton L J, Chrischilles E A, Cooper C, Lane A W, Riggs B L. Perspective. How many women have osteoporosis? J Bone Miner Res 1992; 7 (9): 1005-10.

Mitton D, Cendre E, Roux J P, Arlot M E, Peix G, Rumelhart C, Babot D, Meunier P J. Mechanical properties of ewe vertebral cancellous bone compared with histomorphometry and high-resolution computed tomography parameters. Bone 1998; 22: 651-8.

Mosekilde L. Normal vertebral body size and compressive strength: relations to age and to vertebral and iliac trabecular bone compressive strength. Bone 1986; 7 (3): 207-12.

Mosekilde L, Danielsen C C. Biomechanical competence of vertebral trabecular bone in relation to ash density and age in normal individuals. Bone 1987; 8 (2): 79-85.

Mueller K H, Trias A, Ray R D. Bone density and compositon. Age-related and pathological changes in water and mineral content. J Bone Joint Surg [Am] 1966; 48 (1): 140-8.

Muller R, Hahn M, Vogel M, Delling G, Ruegsegger P. Morphometric analysis of noninvasively assessed bone biopsies: comparison of high-resolution computed tomography and histologic sections. Bone 1996; 18 (3): 215-20.

Muller R, Van Campenhout H, Van Damme B, Van Der Perre G, Dequeker J, Hildebrand T, Ruegsegger P. Morphometric analysis of human bone biopsies: a quantitative structural comparison of histological sections and microcomputed tomography. Bone 1998; 23 (1): 59-66.

Oleksik A, Ott S M, Vedi S, Bravenboer N, Compston J, Lips P. Bone structure in patients with low bone mineral density with or without vertebral fractures . J Bone Miner Res 2000; 15 (7): 1368-75.

Oxlund H, Mosekilde L, Ortoft G. Reduced concentration of collagen reducible cross links in human trabecular bone with respect to age and osteoporosis. Bone 1996; 19 (5): 479-84.

Parfitt A M. Bone remodeling: Relationship to the amount and structure of bone, and the pathogenesis and prevention of fractures. In: Osteoporosis: Etiology, diagnosis, and managment (Eds.B L Riggs and L J Melton). Raven Press. New York: 1988; 2: 45-93.

Parfitt A M, Drezner M K, Glorieux F H, Kanis J A, Malluche H, Meunier P J, Ott S M, Recker R R. Bone histomorphometry: standardization of nomenclature, symbols, and units. Report of the ASBMR Histomorphometry Nomenclature Committee. J Bone Miner Res 1987; 2: 595-610.

Parfitt A M, Han Z H, Palnitkar S, Rao D S, Shih M S, Nelson D. Effects of ethnicity and age or menopause on osteoblast function, bone mineralization, and osteoid accumulation in iliac bone. J Bone Miner Res 1997; 12 (11): 1864-73.

Parfitt A M, Mathews C H, Villanueva A R, Kleerekoper M, Frame B, Rao D S. Relationships between surface, volume, and thickness of iliac trabecular bone in aging and in osteoporosis. Implications for the microanatomic and cellular mechanisms of bone loss. J Clin Invest 1983; 72 (4): 1396-409.

Passoja K, Rautavuoma K, Ala-Kokko L, Kosonen T, Kivirikko K I. Cloning and characterization of a third human lysyl hydroxylase isoform. Proc Natl Acad Sci U S A 1998; 95 (18): 10482-6.

Pistoia W, Van Rietbergen B, Laib A, Ruegsegger P. High-resolution three-dimensional-pQCT images can be an adequate basis for in-vivo microFE analysis of bone. J Biomech Eng 2001; 123 (2): 176-83.

Puustjarvi K, Nieminen J, Rasanen T, Hyttinen M, Helminen H J, Kroger H, Huuskonen J, Alhava E, Kovanen V . Do more highly organized collagen fibrils increase bone mechanical strength in loss of mineral density after one-year running training? J Bone Miner Res 1999; 14 (3): 321-9.

Recker R R. Architecture and vertebral fracture. Calcif Tissue Int 1993; 53 (Suppl 1): S139-S142

Robey P G, Boskey A L. The biochemistry of bone. In: Osteoporosis (Eds.R Marcus, D Feldman, J P Bilezikian, and J Kelsey). Academic Press. New York: 1995: 95-183.

Ross P D, Davis J W, Epstein R S, Wasnich R D. Pre-existing fractures and bone mass predict vertebral fracture incidence in women. Ann Intern Med 1991; 114 (11): 919-23.

Rossert R, de Crombrugghe B. Type I collagen: structure, synthesis and regulation. In: Principles of bone biology (Eds.J P Bilezikian, L G Raisz, and G A Rodan). Academic Press. San Diego: 1996; 10: 127-42.

Schenk R K, Olah A J, Herrmann W. Preparation of calcified tissues for light microscopy. In: Methods in calcified tissue preparation (Ed.G R Dickson). Elsevier. New York: 1984: 1-56.

Scott J E, Hughes E W, Shuttleworth A. A collagen-associated Ehrlich chromogen: A pyrrolic crosslink. Biosc Rep 1981; 1: 611-8.

Seeley D G, Browner W S, Nevitt M C, Genant H K, Scott J C, Cummings S R. Which fractures are associated with low appendicular bone mass in elderly women? The Study of Osteoporotic Fractures Research Group. Ann Intern Med 1991; 115 (11): 837-42.

Sims T J, Avery N C, Bailey A J. Quantitative determination of collagen cross-links. Methods in Molecular Biology vol 139. In: Extracellular matrix protocol (Eds. C Streuhli and M E Grant). Humana Press. New York: 2000: 11-26.

Sims T J, Bailey A J. Quantitative analysis of collagen and elastin cross-links using a single-column system. J Chromatogr 1992; 582 (1-2): 49-55.

Singer K, Edmondston S, Day R, Breidahl P, Price R. Prediction of thoracic and lumbar vertebral body compressive strength: correlations with bone mineral density and vertebral region. Bone 1995; 17 (2): 167-74.

Snyder B D, Piazza S, Edwards W T, Hayes W C. Role of trabecular morphology in the etiology of age-related vertebral fractures. Calcif Tissue Int 1993; 53 (Suppl. 1): S14-S22.

Thomsen J S, Ebbesen E N, Mosekilde L. Relationships between static histomorphometry and bone strength measurements in human iliac crest bone biopsies. Bone 1998; 22: 153-63.

Triffitt J T. The organic matrix of bone tissue. In: Fundamental and clinical bone physiology (Ed.M Urist). Lippincott. Philadelphia: 1980; 3: 45-82.

Turner C H, Hsieh Y F, Muller R, Bouxsein M L, Rosen C J, McCrann M E, Donahue L R, Beamer W G. Variation in bone biomechanical properties, microstructure, and density in BXH recombinant inbred mice. J Bone Miner Res 2001; 16 (2): 206-13.

Ulrich D, Van Rietbergen B, Laib A, Ruegsegger P. The ability of three-dimensional structural indices to reflect mechanical aspects of trabecular bone. Bone 1999; 25 (1): 55-60.

Van Rietbergen B, Majumdar S, Pistoia W, Newitt D C, Kothari M, Laib A, Ruegsegger P. Assessment of cancellous bone mechanical properties from micro-FE models based on micro-CT, pQCT and MR images. Technol Health Care 1998; 6 (5-6): 413-20.

Vater C A, Harris E D J, Siegel R C. Native cross-links in collagen fibrils induce resistance to human synovial collagenase. Biochem J 1979; 181 (3): 639-45.

Vesterby A. Star volume of marrow space and trabeculae in iliac crest: sampling procedure and correlation to star volume of first lumbar vertebra. Bone 1990; 11: 149-55.

Von der Mark K. Structure, Biosynthesis, and gene regulation of collagens in cartilage and bone. In: Dynamics of bone and cartilage metabolism (Eds. M J Seibel, S P Robins, and J P Bilezikian). Academic Press. San Diego: 1999; 1: 3-29.

Weaver J K, Chalmers J. Cancellous bone: its strength and changes with aging and an evaluation of some methods for measuring its mineral content. J Bone Joint Surg [Am] 1966; 48 (2): 289-98.

Wenzel T E, Schaffler M B, Fyhrie D P. In vivo trabecular microcracks in human vertebral bone. Bone 1996; 19 (2): 89-95.